Effects of Short-Range Correlations on the Coulomb Screening and the Pairing Interactions in Electron-Phonon Systems – Triplet Pairing Mediated by Phonons –

Hiroshi SHIMAHARA

Department of Quantum Matter Science, ADSM, Hiroshima University, Higashi-Hiroshima 739-8530, Japan

(Received March   , 2004)

Effects of short-range correlations on the Coulomb screening, the phonons, and the pairing interactions are examined in electron-phonon systems. First, we derive a model Hamiltonian of Coulomb interactions which includes both the long-range part v_q and the short-range part U. It is found from the expression of the dielectric function that the strong on-site correlations weaken the Coulomb screening. Secondly, we examine the screened phonons and the interaction mediated by phonons. In a consistent picture, we derive an expression of the effective interaction which includes (1) the screened Coulomb interactions, (2) the pairing interactions mediated by phonons, and (3) the effective interactions mediated by spin and charge fluctuations. It is rewritten in a form of a summation of (a) the effective interactions of the pure Hubbard model without the long-range Coulomb interactions, and (b) the phonon-mediated interactions plus screened Coulomb interactions with corrections due to both U and v_q. Thirdly, we derive an effective Hamiltonian analogous to the BCS Hamiltonian. Fourthly, for some typical values of parameters, we obtain the ground state phase diagrams. It is found that spin-triplet superconductivity mediated by phonons occurs when the short-range electron correlations are sufficiently strong, and the Coulomb screening is sufficiently weak. We estimate the orders of the transition temperatures when the triplet superconductivity occurs. The obtained values are realistic for existing candidates of the triplet superconductors as the order of the magnitudes. The possible relevance of the phonon-mediated interactions to the heavy fermion superconductor UPt_3 and the layered superconductors such $(TMTSF)_2X$ and Sr_2RuO_4 are briefly discussed.

KEYWORDS: phonon-mediated pairing interactions, Coulomb screening, electron-phonon system, overscreening, spin and charge fluctuations, exotic superconductors, spin-triplet pairing, heavy fermion superconductors, organic superconductors, ruthenate superconductors.

1.   Introduction

It is widely known that overscreening of the repulsive Coulomb interactions between electrons by ions gives rise to attractive interactions for low frequencies $|\omega| \lesssim \omega_D$.[1] This dynamical effect is considered to be the origin of the pairing interactions mediated by phonons, which induce the superconductivity in metals. At the same time, the long-range Coulomb interactions are screened into short-range interactions, and consequently the energies of the optical phonons of short wavelengths are reduced into the accoustic type $\omega_q \sim |\boldsymbol{q}|$.

On the other hand, the screening of electronic and ionic charges influences the momentum dependence of the attractive interactions through the dielectric function. If there were not the screening, the coupling constant between electrons and optical phonons diverges as $|\boldsymbol{q}| \to 0$ due to the long-range nature of the Coulomb interactions. However, in actuality, such divergence is suppressed by the screening, but the coupling constant remains momentum dependent.

Owing to such momentum dependences of the electron-phonon coupling constant and the phonon energy, the resultant pairing interaction mediated by phonons depends on the momentum transfer. Hence, it includes the anisotropic components, when it is expanded in terms of appropriate basis functions. Usually, such anisotropic components are ignored, because they are considered to be much smaller than the isotropic component in most cases. In fact, the superconductivity in the ordinary metals, which are probably mediated by phonons, are considered to be of s-wave pairing.

However, as Foulkes and Gyorffy pointed out,[2] when the short-range Coulomb interactions are strong enough to suppress isotropic pairing, anisotropic pairing can be induced by the subdominant anisotropic interaction. They have examined possibility of spin-triplet superconductivity by this mechanism in metals such as Rh, W, and Pd.

Abrikosov discussed high-T_c cuprates, and proposed that such momentum dependence of the phonon-mediated pairing interaction could give rise to extended s-wave superconductivity,[3] although it seems from some experiments that the cuprates are d-wave superconductors. Following his theory, Bouvier and Bok calculated the superconducting gap function and obtained anisotropic momentum dependence.[4] Friedel and

Kohmoto, and Chang, Friedel and Kohmoto examined the d-wave pairing interactions mediated by phonons in the cuprates.[5, 6] The present author and Kohmoto have proposed[7] that in the presence of coexisting ferromagnetic long-range order, a subdominant triplet state occurs after the singlet states are suppressed by the strong exchange field. We have discussed a possibility of this mechanism in UGe$_2$.[8, 9]

It is easily verified that the momentum dependence of the interaction is stronger for weaker screening. For example, in the Thomas-Fermi approximation, the coupling constant has a peak with the width of the inverse screening length in the momentum space. Therefore, in the interactions, the ratios of the anisotropic components to the isotropic component increase[10] when the screening becomes weaker. There are some possible factors which weaken the screening effect, such as crystal structures, low density of charge carriers, and low density of states. The present author and Kohmoto have examined layer structures as the weakening mechanism,[11] because some candidates of the triplet superconductors have layer structures as we shall discuss below. It was found that when the layer interval increases, the screening becomes weaker, and subdominant triplet pairing interaction could more easily overcome the dominant s-wave pairing interaction with an asist of the on-site Coulomb repulsion.

It should be noted[7, 11] that the on-site Coulomb interaction is specific to the electron systems in solid, and does not appear in the electron gas model in the continuum space. The magnitude of the on-site Coulomb energy U depends on the profile of the Wannier functions. Since such an on-site interaction is constant in the crystal momentum space, it only suppresses isotropic pairing, and consequently it favors subdominant anisotropic pairing.[11]

With respect to application, we are motivated by recently discovered exotic superconductors, such as Sr$_2$RuO$_4$, organic superconductors, and heavy fermion superconductors. In the Sr$_2$RuO$_4$ superconductor, spin-triplet pairing has been suggested by a Knight shift measurement[12] and a μSR experiment.[13] Many theories have been proposed on this material, and there are some controversies especially on the momentum dependence of the superconducting gap function.[14] Particularly, some nonphonon mechanisms have been considered,[14] but there has not been any evidence at present. On the other hand, the Sr$_2$RuO$_4$ superconductor exhibited the isotope effect coefficients with unusual dependence on the impurity (or oxygen defect) concentration and a reverse isotope effect in clean samples.[15] The formar can be explained by assuming internal transition of superconductivity,[16] if the phonon-mediated pairing interaction exists. For the latter result, it has been shown[17] that within the weak coupling theory, the reverse isotope effect indicates that the Coulomb interaction between electrons, in total effect, works as repulsive interactions against the superconduc-

tivity, unless the system is in the very vicinity of any magnetic instability. At present, any pure nonphonon theory could not explain these experimental facts of the isotope effect.

Another candidate of the present mechanism of triplet superconductivity is the family of (TMTSF)$_2$X compounds. From the experimental results at the early stage after the discovery of superconductivity in these compounds, including nuclear magnetic resonance (NMR)[18, 19] and the phase diagrams,[20] d-wave superconductivity mediated by antiferromagnetic spin fluctuation has been studied in these compounds.[21, 22] However, recent experimental studies suggest spin-triplet superconductivity in (TMTSF)$_2$PF$_6$[23] and (TMTSF)$_2$ClO$_4$,[24, 25] although some of the experimental results have not been explained by triplet pairing.[26] We will examine this problem in a separate paper in details, applying the present mechanism of triplet pairing to these compounds.[27] Only by the phonon mechanism, it might be difficult to reproduce the pressure dependence of the superconducting transition temperature T_c observed in these compounds.[20] The pressure dependence may be explained by taking into account the contribution from the spin fluctuations to the pairing interactions. The pairing interactions mediated by the spin fluctuations include the attractive triplet components.[22, 28]

We also consider the heavy fermion superconductors, such as UPt$_3$,[29, 30] as candidates in which the pairing interactions mediated by phonons may contribute to spin-triplet pairing. Since the width of the effective band is extremely narrow, s-wave state could not avoid the on-site Coulomb repulsion by the retardation effect. If one use the Thomas-Fermi approximation in the estimation of the screening length, it becomes much smaller than the lattice constant. However, it is not justified for a phenomena of such a small length scale. In actuality, the dipole field due to the charge distributions in the unit cell could not decay so rapidly within the scale of the lattice constant. Hence, the electron-ion interaction is not necessarily limited on the each lattice site. Therefore, it may contribute to the anisotropic pairing interactions. Whatever the pairing mechanism is, since the heavy mass renormalization significantly reduces the effective coupling constant of the pairing interaction, the bare pairing interaction needs to be very large for the observed T_c to be reproduced.

In general, it is reasonable that the phonon-mediated pairing interaction could contribute to superconductivity to some extent in most cases, even when the resultant gap function is anisotropic. In fact, in almost all superconductors including exotic ones, non-vanishing isotope effects have been observed. It is reasonable to take them due to attractive contributions from phonons to the pairing interactions. It is likely that the momentum average like $\langle \gamma^*(\boldsymbol{k}) V_{\mathrm{ph}}(\boldsymbol{k} - \boldsymbol{k}') \gamma(\boldsymbol{k}') \rangle$ is negative, since the phonon-mediated pairing interaction $V_{\mathrm{ph}}(\boldsymbol{q})$ have a negative peak

around $\boldsymbol{q} = 0$ and $|\gamma(\boldsymbol{k})|^2 > 0$, where $\gamma(\boldsymbol{k})$ denotes the function that expresses the momentum dependence of the gap function $\Delta(\boldsymbol{k}) \propto \gamma(\boldsymbol{k})$. Further, it is likely that the isotropic component is dominant, and the second and third-dominant ones are anisotropic and of odd and even parities in the momentum space, respectively.

In particular, in the spin-triplet superconductors, the phonon-mediated pairing interaction can be the main mechanism of the anisotropic superconductivity, although another mechanism might assist it at the same time.[31] By an analogy to the superfluidity in liquid ^{3}He,[32] the paramagnon mechanism is sometimes considered to be responsible for the spin-triplet superconductivity. However, the situation is very different from the electron systems in the solids. The liquid ^{3}He does not have lattice vibrations, and its transition temperature is of the order of 1mK.[33] Therefore, we should be careful when we use the analogy.

In the anisotropic singlet superconductors, the third-dominant component of the phonon-mediated interaction may contribute to the superconductivity to some extent. However, we presume that it could not be the only origin of the pairing interaction. If the pairing interaction of nonphonon origin is negligible, the system should undergo a transition to triplet superconductivity at a higher temperature, since the third-dominant even-parity (spin-singlet) component is smaller than the second-dominant odd-parity (spin-triplet) component.

In this paper, we examine the effects of the short-range (on-site) correlations on the Coulomb screening, phonons, and the pairing interactions, taking into account the long-range Coulomb interactions at the same time. The main purpose of this paper is to devolop a general theory, although we are motivated by the superconductors discussed above. In particular, we derive a general effective Hamiltonian in a unified framework in which the short-range and long-range parts of the Coulomb interactions are treated consistently. The effective Hamiltonian includes (1) the screened Coulomb interactions, (2) the phonon-mediated interactions by the screened electron-phonon interactions, and (3) the effective interactions mediated by spin and charge fluctuations. In appropriate limits, it is reduced to the effective Hamiltonians examined by many authors so far.[3–7,11] In particular, in our previous papers, the on-site Coulomb energy U has been treated as a parameter independent of the phonon-mediated pairing interaction, but in practice it also modifies the pairing interactions. We will also clarify it in this paper.

In §2, we examine the model of the electron-phonon system. Starting from a basic model of the electron-phonon system, we derive a Hamiltonian which includes both the short-range part U and the long-range part $v_{\boldsymbol{q}}$ of the Coulomb interactions. In §3, we apply the random phase approximation (RPA) to the Hamiltonian obtained in §2, and examine the screening effects on the Coulomb interactions and phonons. The approximation is reduced

to that in the electron gas model if we put $U = 0$ and $v_{\boldsymbol{q}} \neq 0$, while that in the pure Hubbard model if we put $U \neq 0$ and $v_{\boldsymbol{q}} = 0$. In §4, we examine the two-particle vertex part which contributes to superconductivity. We derive the general form which includes corrections due to U as mentioned above. In §5, we derive an effective interaction within the weak coupling theory from the results of §4. We examine anisotropic superconductivity on the basis of the effective interaction. Expressions of the transition temperature and the isotope effect coefficient are derived. In §6, we apply the effective model to some typical cases to clarify essential aspects of the present mechanism. The phase diagrams and the transition temperatures are obtained. The last section §7 is devoted to summary and discussion.

2. A Model of the Electron-Phonon System

In this section, we derive a model that we will examine in this paper. We start with the general form of the coupled electron-phonon Hamiltonian

$$H = H_0 + H_{\text{e-ph}} + H_{\text{C}} \tag{2.1}$$

with

$$H_0 = \sum_{\boldsymbol{k}\sigma} \epsilon_{\boldsymbol{k}} c_{\boldsymbol{k}\sigma}^\dagger c_{\boldsymbol{k}\sigma} + \sum_{\boldsymbol{q}\lambda} \Omega_{\boldsymbol{q}\lambda} b_{\boldsymbol{q}\lambda}^\dagger b_{\boldsymbol{q}\lambda} \tag{2.2}$$

$$H_{\text{e-ph}} = \sum_{\boldsymbol{k}\boldsymbol{q}\sigma\lambda} M_{\boldsymbol{k}\boldsymbol{q}\lambda} c_{\boldsymbol{k}+\boldsymbol{q}\sigma}^\dagger c_{\boldsymbol{k}\sigma} (b_{\boldsymbol{q}\lambda} + b_{-\boldsymbol{q}\lambda}^\dagger) \tag{2.3}$$

$$H_{\text{C}} = \frac{1}{2} \sum_{\substack{\boldsymbol{k}_1 \cdots \boldsymbol{k}_4 \\ \sigma\sigma'}} V_{\boldsymbol{k}_1\boldsymbol{k}_2\boldsymbol{k}_3\boldsymbol{k}_4}^{\sigma\sigma'} c_{\boldsymbol{k}_1\sigma}^\dagger c_{\boldsymbol{k}_2\sigma} c_{\boldsymbol{k}_3\sigma'}^\dagger c_{\boldsymbol{k}_4\sigma'}. \tag{2.4}$$

Here, $c_{\boldsymbol{k}\sigma}$ denotes the electron operator of the Bloch state with the crystal momentum $\boldsymbol{k}$ and the spin σ in the relevant electron band, while $b_{\boldsymbol{q}\lambda}$ denotes the bare phonon operator of the phonon with the momentum $\boldsymbol{q}$ and the phonon-mode λ. Since we consider the longitudinal optical phonons in this paper, we omit the phonon-mode suffix λ and the summation over it for simplicity. Thus, we put $\Omega_{\boldsymbol{q}\lambda} = \Omega_{\text{p}}$, where Ω_{p} denotes the ionic plasma frequency. We consider the positive background charge of the atoms within the jellium model.[1] Therefore, we put the matrix element of the electron-phonon interaction $M_{\boldsymbol{k}\boldsymbol{q}\lambda} = M_{\boldsymbol{q}}$ which satisfies

$$\frac{2M_{\boldsymbol{q}}^2}{\hbar\Omega_{\text{p}}} = \frac{4\pi e^2}{V_{\text{cell}}\boldsymbol{q}^2}, \tag{2.5}$$

where V_{cell} denotes the unit cell volume. The present model might not be very accurate, but since we need an order estimation at most for our purpose, we use this model in this paper for simplicity.

The coupling constant $V_{\boldsymbol{k}_1 \boldsymbol{k}_2 \boldsymbol{k}_3 \boldsymbol{k}_4}^{\sigma\sigma'}$ is expressed as

$$
V_{\boldsymbol{k}_1 \boldsymbol{k}_2 \boldsymbol{k}_3 \boldsymbol{k}_4}^{\sigma\sigma'} = \int \mathrm{d}^3 \boldsymbol{r}\, \mathrm{d}^3 \boldsymbol{r}'\, \psi_{\boldsymbol{k}_1 \sigma}^*(\boldsymbol{r})\, \psi_{\boldsymbol{k}_2 \sigma}(\boldsymbol{r})
$$
$$
\times \frac{e^2}{|\boldsymbol{r} - \boldsymbol{r}'|} \psi_{\boldsymbol{k}_3 \sigma'}^*(\boldsymbol{r}')\, \psi_{\boldsymbol{k}_4 \sigma'}(\boldsymbol{r}')
\tag{2.6}
$$

in terms of the Bloch wave functions

$$
\psi_{\boldsymbol{k}}(\boldsymbol{r}) = \mathrm{e}^{\mathrm{i}\boldsymbol{k}\cdot\boldsymbol{r}} u_{\boldsymbol{k}}(\boldsymbol{r}),
\tag{2.7}
$$

where $u_{\boldsymbol{k}}(\boldsymbol{r})$ satisfies the periodicity condition $u_{\boldsymbol{k}}(\boldsymbol{r} + \boldsymbol{R}) = u_{\boldsymbol{k}}(\boldsymbol{r})$ for any lattice vector $\boldsymbol{R}$, according to the Bloch's theorem.

2.1 An expression in the tight-binding model

Now, we rewrite the Coulomb interaction H_{C} in the tight-binding model. When the tight-binding approximation is valid and the electron wave function has a large amplitude only near the atomic site, we may assume that

$$
\psi_{\boldsymbol{k}}(\boldsymbol{r}) = \frac{1}{\sqrt{N}} \sum_{\boldsymbol{R}} \mathrm{e}^{\mathrm{i}\boldsymbol{k}\cdot\boldsymbol{R}} \phi(\boldsymbol{r} - \boldsymbol{R}),
\tag{2.8}
$$

where $\phi(\boldsymbol{r} - \boldsymbol{R})$ denotes a localized orbital wave function near the atomic site at $\boldsymbol{R}$. This approximation is equivalent to putting

$$
u_{\boldsymbol{k}}(\boldsymbol{r}) = \frac{1}{\sqrt{N}} \sum_{\boldsymbol{R}} \mathrm{e}^{-\mathrm{i}\boldsymbol{k}\cdot(\boldsymbol{r}-\boldsymbol{R})} \phi(\boldsymbol{r} - \boldsymbol{R}).
\tag{2.9}
$$

Since we may put $\boldsymbol{r} \approx \boldsymbol{R}$ in eq. (2.9), it is equivalent also to $u_{\boldsymbol{k}}(\boldsymbol{r}) \approx N^{-1/2} \sum_{\boldsymbol{R}} \phi(\boldsymbol{r}-\boldsymbol{R})$. If we define the Wannier function

$$
w(\boldsymbol{r} - \boldsymbol{R}) = \frac{1}{\sqrt{N}} \sum_{\boldsymbol{k}} \mathrm{e}^{-\mathrm{i}\boldsymbol{k}\cdot\boldsymbol{R}} \psi_{\boldsymbol{k}}(\boldsymbol{r}),
\tag{2.10}
$$

we obtain $w(\boldsymbol{r}) = \phi(\boldsymbol{r})$ from eq. (2.8).

Within this approximation, we obtain

$$
V_{\boldsymbol{k}_1 \boldsymbol{k}_2 \boldsymbol{k}_3 \boldsymbol{k}_4}^{\sigma\sigma'} = \frac{1}{N^2} \sum_{\boldsymbol{R}\boldsymbol{R}'} \int \mathrm{d}^3 \boldsymbol{r}\, \mathrm{d}^3 \boldsymbol{r}'\, |\phi(\boldsymbol{r} - \boldsymbol{R})|^2
$$
$$
\times |\phi(\boldsymbol{r}' - \boldsymbol{R}')|^2\, \mathrm{e}^{-\mathrm{i}(\boldsymbol{k}_1 - \boldsymbol{k}_2)\cdot\boldsymbol{R}} \frac{e^2}{|\boldsymbol{r} - \boldsymbol{r}'|} \mathrm{e}^{-\mathrm{i}(\boldsymbol{k}_3 - \boldsymbol{k}_4)\cdot\boldsymbol{R}'},
\tag{2.11}
$$

where we have omitted terms including the factor of the form $\phi(\boldsymbol{r}-\boldsymbol{R}_1)\phi(\boldsymbol{r}-\boldsymbol{R}_2)$ with $\boldsymbol{R}_1 \neq \boldsymbol{R}_2$, since it is small from the assumption mentioned above. In the integrand of eq. (2.11), we could replace $\boldsymbol{r}$ and $\boldsymbol{r}'$ in $e^2/|\boldsymbol{r} - \boldsymbol{r}'|$ with $\boldsymbol{R}$ and $\boldsymbol{R}'$, respectively, due to the factors of $|\phi(\boldsymbol{r} - \boldsymbol{R})|^2 |\phi(\boldsymbol{r}' - \boldsymbol{R}')|^2$, except when $\boldsymbol{R} = \boldsymbol{R}'$. We could not make this replacement when $\boldsymbol{R} = \boldsymbol{R}'$, because $e^2/|\boldsymbol{r}-\boldsymbol{r}'|$ diverges when $\boldsymbol{r} \to \boldsymbol{r}'$. Therefore, we obtain

$$
V_{\boldsymbol{k}_1 \boldsymbol{k}_2 \boldsymbol{k}_3 \boldsymbol{k}_4}^{\sigma\sigma'} = (U\bar{\delta}_{\sigma\sigma'} + v_{\boldsymbol{k}_1 - \boldsymbol{k}_2})\delta_{\boldsymbol{k}_1 - \boldsymbol{k}_2, \boldsymbol{k}_3 - \boldsymbol{k}_4},
\tag{2.12}
$$

with $\bar{\delta}_{\sigma\sigma'} = 1 - \delta_{\sigma\sigma'}$, where we have defined

$$
U = \int \mathrm{d}^3 \boldsymbol{r}\, \mathrm{d}^3 \boldsymbol{r}'\, |\phi(\boldsymbol{r})|^2 \frac{e^2}{|\boldsymbol{r} - \boldsymbol{r}'|} |\phi(\boldsymbol{r}')|^2,
\tag{2.13}
$$

and

$$
v_{\boldsymbol{q}} = \sum_{\boldsymbol{\rho}\neq 0} \frac{e^2}{|\boldsymbol{\rho}|} \mathrm{e}^{-\mathrm{i}\boldsymbol{q}\cdot\boldsymbol{\rho}}
\tag{2.14}
$$

for $\boldsymbol{q} \neq 0$. It is obvious that the on-site Coulomb energy U depends on the profile of the Wannier function, which expresses the charge distribution near the atomic site. Here, we put $v_{\boldsymbol{q}=0} = 0$, taking into account the charge neutrality in the present jellium model. We call the on-site U and the inter-site $v_{\boldsymbol{q}}$ the short-range and long-range parts of the Coulomb interaction, respectively. If we put $v_{\boldsymbol{q}} = 0$, the present model is reduced to the pure Hubbard model on a lattice, while if we put $U = 0$, it is reduced to the electron gas model in the continuum space except that the momenta are replaced with the crystal momenta.

It is convenient to write eq. (2.4) with matrices as

$$
H_{\mathrm{C}} = \frac{1}{2N} \sum_{\boldsymbol{q}\sigma\sigma'} n_{\boldsymbol{q}\sigma} \Big[v_{\boldsymbol{q}}\hat{\sigma}_0 + (v_{\boldsymbol{q}} + U)\hat{\sigma}_1 \Big]_{\sigma\sigma'} n_{\boldsymbol{q}\sigma'}
$$
$$
= \frac{1}{2N} \sum_{\boldsymbol{q}} \begin{pmatrix} n_{\boldsymbol{q}\uparrow} & n_{\boldsymbol{q}\downarrow} \end{pmatrix} \hat{V}_{\boldsymbol{q}} \begin{pmatrix} n_{\boldsymbol{q}\uparrow} \\ n_{\boldsymbol{q}\downarrow} \end{pmatrix},
\tag{2.15}
$$

where we have introduced the Pauli matrices and the unit matrix, $\hat{\sigma}_1$, $\hat{\sigma}_2$, $\hat{\sigma}_3$, and $\hat{\sigma}_0$, respectively. Here, we have defined $n_{\boldsymbol{q}\sigma} = \sum_{\boldsymbol{k}} c_{\boldsymbol{k}\sigma}^\dagger c_{\boldsymbol{k}+\boldsymbol{q}\sigma}$ and

$$
\hat{V}_{\boldsymbol{q}} \equiv \begin{pmatrix} v_{\boldsymbol{q}} & v_{\boldsymbol{q}} + U \\ v_{\boldsymbol{q}} + U & v_{\boldsymbol{q}} \end{pmatrix}.
\tag{2.16}
$$

We could also rewrite eq. (2.4) as

$$
H_{\mathrm{C}} = \frac{1}{N} \sum_{\boldsymbol{q}} \Big[\frac{1}{2}(v_{\boldsymbol{q}} + \frac{U}{2}) n_{\boldsymbol{q}} n_{-\boldsymbol{q}} - U S_{\boldsymbol{q}}^z S_{-\boldsymbol{q}}^z \Big]
\tag{2.17}
$$

with $n_{\boldsymbol{q}} = n_{\boldsymbol{q}\uparrow} + n_{\boldsymbol{q}\downarrow}$ and $S_{\boldsymbol{q}}^z = (n_{\boldsymbol{q}\uparrow} - n_{\boldsymbol{q}\downarrow})/2$.

2.2 Approximation for the long-range part

Now, we examine the long-range parts $v_{\boldsymbol{q}}$ in detail. For small $\boldsymbol{q} \neq \boldsymbol{0}$, we could approximate $v_{\boldsymbol{q}}$ by

$$
v_{\boldsymbol{q}} \approx \int \frac{e^2}{|\boldsymbol{\rho}|} \mathrm{e}^{-\mathrm{i}\boldsymbol{q}\cdot\boldsymbol{\rho}} \frac{\mathrm{d}^3 \boldsymbol{\rho}}{V_{\mathrm{cell}}} = \frac{4\pi e^2}{V_{\mathrm{cell}}|\boldsymbol{q}|^2}.
\tag{2.18}
$$

Here, we note that a periodicity relation $v_{\boldsymbol{q}+\boldsymbol{K}} = v_{\boldsymbol{q}}$ holds in the original expression eq. (2.14), where $\boldsymbol{K}$ denotes any reciprocal lattice vector, whereas it does not hold in the approximate expression eq. (2.18). Therefore, if one uses eq. (2.18) in calculating the gap function $\Delta(\boldsymbol{k})$, the reciprocal lattice periodicity $\Delta(\boldsymbol{k}) = \Delta(\boldsymbol{k} + \boldsymbol{K})$ of the gap function is broken.

Therefore, we note that the original expression of $v_{\boldsymbol{q}}$, eq. (2.14), is large near $\boldsymbol{q} = \boldsymbol{K}$, not only near $\boldsymbol{q} = 0$, for the lattice periodicity. In the gap equation, the momentum $\boldsymbol{q}$ corresponds to the momentum transfer $\boldsymbol{k} - \boldsymbol{k}'$, where $\boldsymbol{k}$ and $\boldsymbol{k}'$ denote the electron momenta near the Fermi surface. Even when $\boldsymbol{k}$ and $\boldsymbol{k}'$ are in the first Brillouin zone, $\boldsymbol{q} - \boldsymbol{K} = \boldsymbol{k} - \boldsymbol{k}' - \boldsymbol{K}$ can be small, for example when the Fermi surface is open. For such
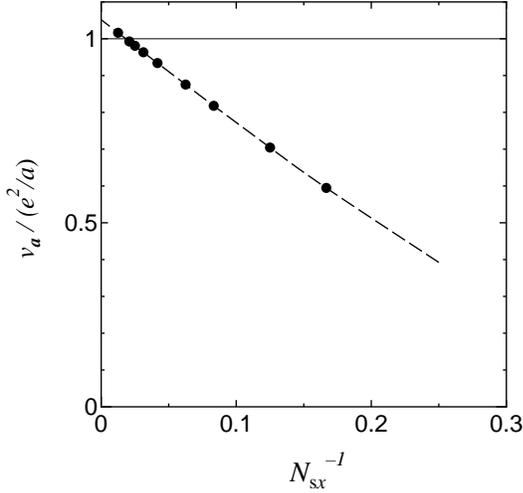
Fig. 1. Estimation of the nearest neighbor Coulomb interaction v_a calculated with the approximate equation (2.19) in the finite size system with the linear dimension N_{sx}. The broken line is the guide for eyes. The thin solid line shows the exact value $v_a = 1$.

k and k', we should use the approximate expression $v_q = 4\pi e^2/V_{\rm cell}|q - K|^2$, which is very different from eq. (2.18) near $q = K$. Therefore, a more appropriate expression of eq. (2.14) is

$$v_q \approx \max_{K}\left[\frac{4\pi e^2}{V_{\rm cell}|q - K|^2}\right] \qquad (2.19)$$

rather than eq. (2.18). This expression is appropriate not only near $q = 0$, but also near $q = K$. Near the Brillouin zone boundary of q, the derivative of the right-hand-side of eq. (2.19) jumps, but since v_q is very small there, it does not cause any difficulty in practice.

Let us examine the error of the above approximation. Since eq. (2.19) becomes exact relation for long wavelengths, it is expected that the error of eq. (2.19) is larger for shorter wavelengths. Hence, the nearest neighbor Coulomb interaction

$$v_a = N^{-1}\sum_{q} v_q {\rm e}^{{\rm i}q_x a} \qquad (2.20)$$

would have the largest error, where $a = (a, 0, 0)$ denotes one of the unit lattice vectors, since the on-site Coulomb interaction U is not included in the definition of v_q, eq. (2.14). Figure 1 shows the result of eq. (2.20) calculated with the approximate equation (2.19) in the electron system on the cubic lattice with the number of the lattice sites $N = N_{sx}^3$, where N_{sx} denotes the number of the lattice sites in one direction. It is found that as the system size increases, the value of v_a estimated by eq. (2.19) approach a value $\approx 1.05 \times e^2/a$, which is only 5% larger than the exact value. Therefore, the present approximation does not cost major error even in the short wavelength behavior.

3. Coulomb Screening

In this section, we examine the screening effects on the Coulomb interactions between two electrons, the electron-phonon interactions, and the phonon propagators. For convenience, we define appropriately scaled functions of the charge and spin fluctuations in the pure Hubbard model *i.e.*, the model with $U \neq 0$ and $v_q = 0$, in the RPA by

$$\chi_{\rm c}^{(0)}(q) = \frac{2\chi_0(q)}{1 + U\chi_0(q)}$$
$$\chi_{\rm s}^{(0)}(q) = \frac{1}{2}\frac{\chi_0(q)}{1 - U\chi_0(q)}, \qquad (3.1)$$

where we have defined

$$\chi_0(q) = -T\sum_{n} N^{-1}\sum_{k} G_{\sigma}^{(0)}(k + q)\, G_{\sigma}^{(0)}(k)$$
$$= N^{-1}\sum_{k}\frac{f(\xi_k) - f(\xi_{k+q})}{{\rm i}\nu_m + \xi_{k+q} - \xi_k} \qquad (3.2)$$

with the unperturbed Green's function $G_{\sigma}^{(0)}$. Here, we have introduced the four-momentum notation such as $q = (q, {\rm i}\nu_m)$ and $k = (k, {\rm i}\omega_n)$.

3.1 Fluctuations and Screened Coulomb Interactions

In this subsection, we derive an expression of the screened Coulomb interactions in the presence of both the short and long-range parts of the Coulomb interactions, U and v_q.

First, we consider the ring diagrams by the RPA as depicted in Fig. 3, where the momenta and spins are assigned as shown in Fig. 2. Since the dashed lines of the Coulomb interactions have the same momentum q in those diagrams, they become divergently large at the same time for small $|q|$. Therefore, this series gives a major contribution for long wavelengths.

The vertex due to the ring diagrams is obtained as

$$\hat{\Gamma}^{\rm ring}(k, k', q) = \hat{V}_q\left[\hat{\sigma}_0 + \chi_0(q)\,\hat{V}_q\right]^{-1} \qquad (3.3)$$

in the matrix form in the spin space. Equation (3.3) is rewritten as

$$\hat{\Gamma}^{\rm ring}(k, k', q) = \frac{1}{2}\frac{2v_q + U}{1 + (2v_q + U)\chi_0(q)}\begin{pmatrix} 1 & 1 \\ 1 & 1 \end{pmatrix}$$
$$+ \frac{1}{2}\frac{-U}{1 - U\chi_0(q)}\begin{pmatrix} 1 & -1 \\ -1 & 1 \end{pmatrix}, \qquad (3.4)$$

and we could put the elements in the form

$$\Gamma_{\sigma\sigma'}^{\rm ring}(k, k', q) = \Gamma_{\rm c}(q) + \Gamma_{\rm s}^{zz}(q)\sigma\sigma'. \qquad (3.5)$$

In the static approximation ${\rm i}\nu_m = 0$, we have the effective

interaction by the ring diagrams

$$
H_{\mathrm{C}}^{\mathrm{ring}} = \frac{1}{N} \sum_{\boldsymbol{q}} \Big[\frac{1}{2} \frac{v_{\boldsymbol{q}} + U/2}{1 + 2(v_{\boldsymbol{q}} + U/2)\chi_0(\boldsymbol{q}, 0)} n_{\boldsymbol{q}} n_{-\boldsymbol{q}}
$$
$$
- \frac{U}{1 - U\chi_0(\boldsymbol{q}, 0)} S_{\boldsymbol{q}}^z S_{-\boldsymbol{q}}^z \Big]. \tag{3.6}
$$

Here, we note that the rotational symmetry in the spin space is not retained if we take only the ring diagrams.[34]

In order to recover the rotational invariance, we need to take the particle-hole ladder diagrams depicted in Fig. 4, with respect to U. The second term in the braket of eq. (3.6) becomes divergently large for the momentum $\boldsymbol{q}$ near the nesting vector $\boldsymbol{Q}$, when the Fermi surface has a good nesting condition, as known in the Hubbard model.[35, 36] It is also known that the contribution from the ladder diagrams in Fig. 4 is of the same order as that from the ring diagrams.

In contrast, in the RPA in the pure electron gas model with $U = 0$, the ladder diagrams are ignored. Since the momentum of the interaction lines do not always coincide as those in the ring diagrams, the contribution from the ladder diagrams is smaller than that from the ring diagrams. Hence, we omit $v_{\boldsymbol{q}}$ in the ladder diagrams also in the present model.

Thus, the contribution from the ladder diagrams is obtained as

$$
\Gamma_{\sigma\sigma'}^{\mathrm{lad}}(k, k', q) = \frac{-U}{1 - U\chi_0(k - k' - q)}(1 - \delta_{\sigma\sigma'}). \tag{3.7}
$$

In the static approximation, we have

$$
H_{\mathrm{C}}^{\mathrm{lad}} = -\frac{1}{2N} \sum_{\boldsymbol{q}} \frac{U}{1 - U\chi_0(\boldsymbol{q}, 0)}(S_{\boldsymbol{q}}^+ S_{-\boldsymbol{q}}^- + S_{\boldsymbol{q}}^- S_{-\boldsymbol{q}}^+), \tag{3.8}
$$

where we have defined

$$
S_{\boldsymbol{q}}^+ = \sum_{\boldsymbol{k}} c_{\boldsymbol{k}\uparrow}^\dagger c_{\boldsymbol{k}+\boldsymbol{q}\downarrow}
$$

and $S_{\boldsymbol{q}}^- = (S_{\boldsymbol{q}}^+)^\dagger$. Adding eqs. (3.6) and (3.8), we obtain a rotationally invariant effective interaction

$$
\tilde{H}_{\mathrm{C}} = \frac{1}{N} \sum_{\boldsymbol{q}} \Big[\frac{1}{2} \frac{v_{\boldsymbol{q}} + U/2}{1 + 2(v_{\boldsymbol{q}} + U/2)\chi_0(\boldsymbol{q}, 0)} n_{\boldsymbol{q}} n_{-\boldsymbol{q}}
$$
$$
- \frac{U}{1 - U\chi_0(\boldsymbol{q}, 0)} \boldsymbol{S}_{\boldsymbol{q}} \cdot \boldsymbol{S}_{-\boldsymbol{q}} - U n_{\boldsymbol{q}\uparrow} n_{-\boldsymbol{q}\downarrow} \Big], \tag{3.9}
$$

where the last term subtracts the double counted contribution of the first order diagrams in Figs. 3 and 4. From eq. (3.9), one could reproduce the vertex parts by the RPA both in the electron gas model and in the Hubbard model by taking appropriate limits, $U \to 0$ and $v_{\boldsymbol{q}} \to 0$, respectively. When we use the effective Hamiltonian of eq. (3.9) in the electron self-energy, we should subtract another double counted contribution from the second terms in Figs. 3 and 4.[36]

Within the same approximation, the propagators for the charge and spin fluctuations are obtained as

$$
\chi_{\mathrm{c}}(q) = \frac{2\chi_0(q)}{1 + (2v_{\boldsymbol{q}} + U)\chi_0(q)}
$$
$$
\chi_{\mathrm{s}}(q) = \frac{1}{2} \frac{\chi_0(q)}{1 - U\chi_0(q)} = \chi_{\mathrm{s}}^{(0)}(q). \tag{3.10}
$$

Hence, we can rewrite eq. (3.9) as

$$
\tilde{H}_{\mathrm{C}} = H_{\mathrm{C}} + H_{\mathrm{cf}} + H_{\mathrm{sf}}, \tag{3.11}
$$

where

$$
H_{\mathrm{cf}} = -\frac{1}{2N} \sum_{\boldsymbol{q} \neq 0} (v_{\boldsymbol{q}} + \frac{U}{2})^2 \chi_{\mathrm{c}}(\boldsymbol{q}, 0) \, n_{\boldsymbol{q}} n_{-\boldsymbol{q}}
$$
$$
H_{\mathrm{sf}} = -\frac{1}{2N} \sum_{\boldsymbol{q} \neq 0} 4U^2 \chi_{\mathrm{s}}(\boldsymbol{q}, 0) \, \boldsymbol{S}_{\boldsymbol{q}} \cdot \boldsymbol{S}_{-\boldsymbol{q}}. \tag{3.12}
$$

The terms H_{cf} and H_{sf} can be regarded as the interactions mediated by the charge and spin fluctuations, respectively.

3.2 Dielectric function and the screening length

The first terms of eqs. (3.4) and (3.9) are the interactions between the charge degrees of freedom of electrons. Hence, we obtain an expression of the dielectric function

$$
\kappa(q) = 1 + 2(v_{\boldsymbol{q}} + \frac{U}{2})\chi_0(q). \tag{3.13}
$$

In the long wavelength limit $\boldsymbol{q} \to 0$, since $v_{\boldsymbol{q}} \gg U$, we obtain Thomas-Fermi dielectric constant

$$
\kappa(q) = 1 + \frac{q_{\mathrm{TF}}^2}{\boldsymbol{q}^2} \equiv \kappa_{\mathrm{TF}}(q) \tag{3.14}
$$

with $q_{\mathrm{TF}}^2 = 8\pi e^2 N(0)/V_{\mathrm{cell}}$, where $\lambda_{\mathrm{TF}} = 1/q_{\mathrm{TF}}$ and $N(0)$ denote the Thomas-Fermi screening length and the electron density of states at the Fermi energy per a spin and a site. For the short wavelength $|\boldsymbol{q}| \gg q_{\mathrm{s}}$, we can omit $v_{\boldsymbol{q}}$ compared to U,

$$
\kappa(q) = 1 + U\chi_0(q) \equiv \kappa_U(q), \tag{3.15}
$$

which is the result in the Hubbard model.

Equation (3.13) is written in the form,

$$
\kappa(q) = \kappa_U(q)\tilde{\kappa}_v(q), \tag{3.16}
$$

where

$$
\tilde{\kappa}_v(q) = 1 + v_{\boldsymbol{q}}\chi_{\mathrm{c}}^{(0)}(q) = 1 + \frac{\tilde{q}_{\mathrm{s}}^2}{\boldsymbol{q}^2}
$$
$$
\tilde{q}_{\mathrm{s}}^2 = q_{\mathrm{TF}}^2 \frac{\chi_{\mathrm{c}}^{(0)}(q)}{2N(0)} = \frac{q_{\mathrm{s}}^2}{\kappa_U(q)} \tag{3.17}
$$
$$
q_{\mathrm{s}}^2 = q_{\mathrm{TF}}^2 \frac{\chi_0(q)}{N(0)}
$$

with $\chi_{\mathrm{c}}^{(0)}$ defined in eq. (3.1). In the absence of U, in the system with the spherical Fermi surface, eq. (3.16) is reduced to the Lindhard's result of the RPA in the electron gas model.
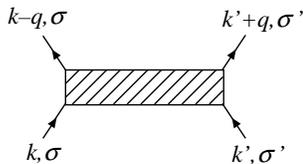
Fig. 2. Assignment of the momenta and spins in the two body vertex part $\Gamma(k, k', q)$.
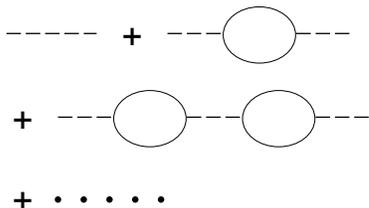
Fig. 3. Summation of the ring diagrams. The solid and broken lines denote the electron Green's function and the Coulomb interaction eq. (2.12).

Fig. 4. Summation of the particle-hole ladder diagrams. The definitions of the lines are the same as those in Fig. 3. The incoming and outgoing thin solid lines are to show how to apply the diagrams to the two-particle vertex in the self-energy and the superconductive gap equation.

Fig. 5. Renormalization of the electron-phonon interaction. The solid lines denote the electron Green's functions, and the closed circle denotes the bare electron-phonon interaction. The thin solid and wavy lines are to show how to apply the diagrams to the electron and phonon Green's functions, respectively. The thick dashed line denotes the screened Coulomb interaction.

For long wavelengths and in the static approximation, we have $\chi_0(q) \approx N(0)$ and $\kappa_U(q) \approx 1 + UN(0)$. Hence, we obtain the screening length

$$\tilde{\lambda}_{\mathrm{scr}} = \lambda_{\mathrm{TF}} \sqrt{\kappa_U(0)} = \lambda_{\mathrm{TF}} \sqrt{1 + \mu_{\mathrm{C}}} \qquad (3.18)$$

from eq. (3.17), where we have put

$$\mu_{\mathrm{C}} = UN(0). \qquad (3.19)$$

Therefore, it is found that the screening length is lengthened by a correlation effect due to the on-site Coulomb repulsion in comparison to the Thomas-Fermi screening length λ_{TF}. It is plausible that the local electron density less easily deviates from the uniform value in the presence of strong correlations. In other words, the charge fluctuations are reduced ($[\chi_{\mathrm{c}}^{(0)}]_{U \neq 0} < [\chi_{\mathrm{c}}^{(0)}]_{U=0}$) and $\kappa_U > 1$, when $U > 0$. It is interesting that the short-range part of the Coulomb interactions affects the long-range behavior through a many body effect.

3.3 Corrections to the electron-phonon interactions

Now, let us examine renormalization of the electron-phonon interaction due to the Coulomb screening effect as depicted in Fig. 5. As the screened Coulomb interaction, we take the series of the ring diagrams shown in Fig. 3. However, if we apply the ladder diagrams in thick dashed line in Fig. 5, the ring part consists of many electron lines. In such a ring, the integrand could be large only in a very small part of the phase space of the in-

tegral variables. Hence, we omit the ladder diagrams for simplicity. This simplification is also justified from the rotational invariance in the spin space. Since we could take the spin summation for the ring part in Fig. 5, the spin interaction in eq. (3.4) vanishes. Thus, the electron-phonon vertex part is not rotationally invariant if we retain the ladder diagrams. Therefore, we ignore them, and obtain the electron-phonon vertex part

$$\tilde{M}(q) = \frac{M_{\boldsymbol{q}}}{\kappa(q)}. \qquad (3.20)$$

3.4 Corrections to the phonons

In this subsection, we examine the phonon Green's function. We consider the renormalization of the phonons due to the Coulomb screening through the electron-phonon interaction shown in Fig. 5. Then, we obtain the diagram equation shown in Fig. 6. This approximation is equivalent to that for the polarization propagator as shown in Fig. 7.
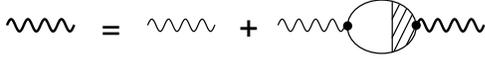
Fig. 6. The diagram equation for the dressed phonon Green's function. The thick and thin wavy lines denote the dressed and bare phonon Green's functions, respectively. The renormalized electron-phonon interaction is shown in Fig. 5.
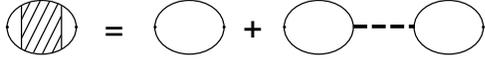
Fig. 7. The diagram equation for the polarization propagator. The solid line and thick dashed line denote the bare electron Green's function and the screened Coulomb interaction.

The phonon Green's function is defined by

$$\mathcal{D}(\boldsymbol{q}, \tau) = -\langle T_\tau \left[\varphi_{\boldsymbol{q}}(\tau) \varphi_{\boldsymbol{q}}^\dagger \right] \rangle \tag{3.21}$$

with $\varphi_{\boldsymbol{q}} = b_{\boldsymbol{q}} + b_{-\boldsymbol{q}}^\dagger$, where we have defined $A(\tau) = e^{\tau H} A e^{-\tau H}$. The bare phonon Green's function $\mathcal{D}_0(\boldsymbol{q}, \tau)$ is defined in a similar manner, and the Fourier transform is expressed as

$$\mathcal{D}_0(\boldsymbol{q}, i\nu_m) = \frac{-2\Omega_{\mathrm{p}}}{\nu_m^2 + \Omega_{\mathrm{p}}^2}. \tag{3.22}$$

The polarization propagator of Fig. 7 summed over spins is expressed as

$$P(q) = 2\chi_0(q) - [\chi_0(q)]^2 \sum_{\sigma\sigma'} (\Gamma_{\mathrm{c}}(q) + \Gamma_{\mathrm{s}}^{zz}(q)\sigma\sigma') \tag{3.23}$$

$$= 2\chi_0(q)/\kappa(q) \equiv \chi_{\mathrm{c}}(q),$$

where $\chi_{\mathrm{c}}(q)$ denotes the charge fluctuations. From Fig. 6 with Fig. 5 and eq. (3.20) or with Fig. 7 and eq. (3.23), we obtain

$$\mathcal{D}(q) = \mathcal{D}_0(q) - \mathcal{D}_0(q) \frac{2M_{\boldsymbol{q}}^2 \chi_0(q)}{\kappa(q)} \mathcal{D}(q), \tag{3.24}$$

and thus

$$\mathcal{D}^{-1} = \mathcal{D}_0^{-1} + M_{\boldsymbol{q}}^2 \chi_{\mathrm{c}}(q). \tag{3.25}$$

Using eqs. (3.22) and (2.5), we obtain

$$\mathcal{D}^{-1} = -\frac{1}{2\Omega_{\mathrm{p}}} \left[\nu_m^2 + [\tilde{\omega}(q)]^2 \right] \tag{3.26}$$

with

$$\tilde{\omega}(q) = \Omega_{\mathrm{p}} \sqrt{\frac{\kappa_U(q)}{\kappa(q)}} = \frac{\Omega_{\mathrm{p}}}{\tilde{\kappa}_v(q)}. \tag{3.27}$$

The renormalized phonon dispersion energy is obtained

by solving $\tilde{\omega}_{\boldsymbol{q}} = \tilde{\omega}(\boldsymbol{q}, \tilde{\omega}_{\boldsymbol{q}})$, where the function $\tilde{\omega}(\boldsymbol{q}, \omega)$ is obtained by the analitic continuation $i\nu_m \rightarrow \omega + i\delta$ from $\tilde{\omega}(\boldsymbol{q}, i\nu_m)$.

In the long wavelength limit $\boldsymbol{q} \rightarrow 0$, we obtain

$$\tilde{\omega}_{\boldsymbol{q}} = \tilde{c}|\boldsymbol{q}| \tag{3.28}$$

with $\tilde{c} = \Omega_{\mathrm{p}}/\tilde{q}_s$. As is widely known, the longitudinal optical phonons are screened by electrons into the accoustic mode with a dispersion energy proportional to $|\boldsymbol{q}|$ as expressed in eq. (3.28). It is easily verified that putting $U = 0$, one could recover all the standard results of the RPA of the electron gas model in the back-ground jellium positive charge.[1] For $U \neq 0$, we find that the electron correlations due to the on-site Coulomb repulsion weaken the screening effect and increase the sound velocity.

4. Superconductivity

In this section, we examine the two-particle vertex part $\Gamma_{\sigma\sigma_1}(k, k')$, which induces superconductivity. We clarify the corrections to the vertex part due to the on-site Coulomb interactions.

4.1 Definition of the effective interactions

The two-particle vertex part $\Gamma_{\sigma\sigma_1}(k, k')$ is defined as one which scatters the pair of two electrons with (k, σ) and $(-k, \sigma_1)$ to that with (k', σ) and $(-k', \sigma_1)$. The gap equation of superconductivity is written as

$$\Delta_{\sigma\sigma_1}(k) = -\sum_{k'} \Gamma_{\sigma\sigma_1}(k, k')$$
$$\times G_\sigma(k') G_{\sigma_1}(-k') \Delta_{\sigma\sigma_1}(k'), \tag{4.1}$$

where we have introduced an abbreviation

$$\sum_{k'} = N^{-1} \sum_{\boldsymbol{k}'} T \sum_{n'} \tag{4.2}$$

and $G_\sigma(k)$ denotes the dressed electron Green's function. The vertex part $\Gamma_{\sigma\sigma_1}$ plays a role of the effective interactions. The gap equation (4.1) includes the dynamical effect by the Matsubara frequency.

The electron self-energy is calculated by

$$\Sigma_\sigma(k) = -\sum_{k'\sigma'} \Gamma_{\sigma\sigma'}^{(\mathrm{N})}(k, k') G_{\sigma'}(k'), \tag{4.3}$$

where $\Gamma_{\sigma\sigma'}^{(\mathrm{N})}$ denotes the appropriate vertex part for the self-energy consistent with $\Gamma_{\sigma\sigma_1}$. The consistency is considered phenomenologically or microscopically with the Ward-Takahashi identity. Equations (4.1) and (4.3) are called Eliashberg equations.

In order to estimate T_{c} accurately, we need to solve the full set of equations. Especially when we consider the spin-fluctuation-mediated superconductivity, since the attractive part of the interactions is much weaker than the repulsive part, the self-energy effect is important.[37] However, since in this paper we are mainly interested in the phonon-mediated pairing interactions, we omit the self-energy renormalization of the electrons from

now on.

We can improve the perturbation theory[38, 39] by including renormalization of the electron Green's function and the vertex corrections in $\Gamma_{\sigma,\sigma_1}(k, k')$. For example, we could take into account the correction to the spin and charge fluctuations from the self-energy effect by replacing $\chi_0(q)$ with $\chi(q)$, as in the renormalized RPA, although it requires heavy numerical calculations.

However, we expect that the most essential diagrams are taken into account in the RPA. Within the RPA, we could reproduce a physical situation that the strong charge and spin fluctuations mediate the pairing interactions. This consideration is partially based on a phenomelogical viewpoint. However, more or less, we could not avoid such a phenomenological consideration in the perturbation theories based on effective Hamiltonians, such as the Hubbard model. In any perturbation theory, we need to ignore almost all diagrams in the infinite series of the perturbation expansion. Taking a particular series of the diagrams can be rigorously justified only in an appropriate limit, but otherwise it is not quantitatively accurate very much. Furthermore, we need to use the effective Hamiltonian, which is usually far simpler than the real materials. Usually, effective Hamiltonians are useful for qualitative study, but are not very precise quantitatively. Therefore, even if we develope a perturbation theory by purely theoretical efforts beyond the RPA, the applicability of the quantitative results to the real materials are limited, unless any qualitatively distinct result is obtained.

4.2　Expression of the effective pairing interactions

In this subsection, we derive the expression of $\Gamma_{\sigma\sigma_1}(k, k')$ from the results of the previous section §3. From the momentum and spin assignment depicted in Fig. 2 that $\Gamma_{\sigma\sigma'}^{\mathrm{ring}}(k, -k, k - k')$ and $\Gamma_{\sigma\sigma'}^{\mathrm{lad}}(k, -k, k - k')$ in eqs. (3.5) and (3.7) contribute to the vertex part $\Gamma_{\sigma\sigma_1}(k, k')$.

The contribution from the charge fluctuations and the screened Coulomb interaction is obtained from eqs. (3.4) and (3.5) as

$$\Gamma_{\mathrm{c}}(q) = \frac{1}{2} \frac{2v_{\boldsymbol{q}} + U}{1 + (2v_{\boldsymbol{q}} + U)\chi_0(q)} = \frac{v_{\boldsymbol{q}} + U/2}{\kappa(q)}, \quad (4.4)$$

where we have put $q = k - k'$. Similarly, the contribution from the spin fluctuations with respect to the S_z component is written as

$$\sigma\sigma_1 \Gamma_{\mathrm{s}}^{zz}(q) = -\frac{\sigma\sigma_1}{2} \frac{U}{1 - U\chi_0(q)}. \quad (4.5)$$

In addition to them, we obtain the effective interaction mediated by phonons

$$\Gamma_{\mathrm{ph}}(q) = [\tilde{M}(q)]^2 \mathcal{D}(q) = \frac{M_{\boldsymbol{q}}^2}{\kappa(q)} \cdot \frac{-2\Omega_{\mathrm{p}}/\kappa(q)}{\nu_m^2 + [\tilde{\omega}(q)]^2} \quad (4.6)$$

with $\tilde{\omega}(q)$ given in eq. (3.27).

The contribution from the spin fluctuations with re-

spect to the S_x and S_y components is obtained from the ladder diagram as

$$\bar{\delta}_{\sigma\sigma_1} \Gamma_{\mathrm{s}}^{+-}(k, k') = \bar{\delta}_{\sigma\sigma_1} \Gamma^{\mathrm{lad}}(k, -k, k - k')$$
$$= \bar{\delta}_{\sigma\sigma_1} \frac{U}{1 - U\chi_0(k + k')}, \quad (4.7)$$

where $\bar{\delta}_{\sigma\sigma_1} = 1 - \delta_{\sigma\sigma_1}$. By the parity of the gap function $\Delta(\boldsymbol{k}, \mathrm{i}\omega_n)$, we could replace the vertex function eq. (4.7) in the gap equation eq. (4.1) with

$$\bar{\delta}_{\sigma\sigma_1} \Gamma_{\mathrm{s}}^{+-}(k, k') = s\bar{\delta}_{\sigma\sigma_1} \frac{U}{1 - U\chi_0(k - k')}, \quad (4.8)$$

where we take the sign $s = +1$ and $s = -1$ for singlet pairing and triplet pairing, respectively.

Collecting the contributions of eqs. (4.4) - (4.8), we obtain the vertex part

$$\Gamma_{\sigma\sigma_1}(k, k') = \Gamma_{\mathrm{c}}(k - k') + \sigma\sigma_1 \Gamma_{\mathrm{s}}^{zz}(k - k')$$
$$+ \Gamma_{\mathrm{ph}}(k - k') + \bar{\delta}_{\sigma\sigma_1} \Gamma_{\mathrm{s}}^{+-}(k, k') \quad (4.9)$$
$$- U\bar{\delta}_{\sigma\sigma_1}.$$

Here, the last term $-U\bar{\delta}_{\sigma\sigma_1}$ is to subtract the double counted contribution as mentioned below eq. (3.9). With a definition

$$\Gamma_{\mathrm{s}}(q) \equiv \frac{1}{2} \frac{U}{1 - U\chi_0(q)}, \quad (4.10)$$

eq. (4.9) can be rewriten as

$$\Gamma_{\sigma\sigma_1} = \Gamma_{\mathrm{c}} - \sigma\sigma_1 \Gamma_{\mathrm{s}} + \Gamma_{\mathrm{ph}} + 2\bar{\delta}_{\sigma\sigma_1} s\Gamma_{\mathrm{s}} - U\bar{\delta}_{\sigma\sigma_1}. \quad (4.11)$$

Therefore, for singlet pairing, the vertex part $\Gamma_{\sigma,\sigma_1}(k, k')$ is expressed as

$$\Gamma_{\mathrm{sp}} = \Gamma_{\mathrm{c}} + 3\Gamma_{\mathrm{s}} + \Gamma_{\mathrm{ph}} - U, \quad (4.12)$$

while for triplet pairing

$$\Gamma_{\mathrm{tp}} = \Gamma_{\mathrm{c}} + \Gamma_{\mathrm{s}} + \Gamma_{\mathrm{ph}}. \quad (4.13)$$

If we put $v_{\boldsymbol{q}} = 0$, the spin and charge fluctuation terms are reduced to the expressions obtained in many articles.[22, 28, 31, 35, 36] Due to the complicated momentum dependence, it can work as an attractive interaction or as a repulsive interaction in the formation of the Cooper pairs, depending on the symmetry of the gap function and the shape of the Fermi surface.

Since we have obtained the expressions of the vertex part eqs. (4.12) and (4.13), it is possible in principle to solve the Eliashberg equations (4.1) and (4.3). However, we leave it for future study, and derive weak coupling effective Hamiltonian in the next section §5.

4.3　Physical interpretation

In this subsection, we rewrite the expressions obtained above for a physical interpretation. We also discuss the expressions in the two limits, $U \to 0$ and $v_{\boldsymbol{q}} \to 0$.

In eq. (4.11), the screened Coulomb interactions and

the phonon-mediated interactions are rewritten as

$$\Gamma_{\mathrm{c}} + \Gamma_{\mathrm{ph}} = \frac{v_{\boldsymbol{q}} + U/2}{\kappa} - \frac{v_{\boldsymbol{q}}}{\kappa \kappa_U} \frac{[\tilde{\omega}(q)]^2}{-\omega^2 + [\tilde{\omega}(q)]^2}$$
$$= \frac{U}{2\kappa_U} + \frac{v_{\boldsymbol{q}}}{\kappa \kappa_U} \frac{\omega^2}{\omega^2 - [\tilde{\omega}(q)]^2}, \quad (4.14)$$

where we have made the analytic continuation $\mathrm{i}\nu_m \to \omega \pm \mathrm{i}\delta$, and put $q = k - k'$.

Therefore, the total two-particle vertex part is given by

$$\Gamma_{\sigma\sigma_1}(q) = \Gamma_U^{(0)} + \frac{v_{\boldsymbol{q}}}{\kappa \kappa_U} \frac{\omega^2}{\omega^2 - [\tilde{\omega}(q)]^2}, \quad (4.15)$$

with $q = k - k'$, where the function $\Gamma_U^{(0)}$ in the first term is nothing but the vertex part in the pure Hubbard model, *i.e.*, the model with $U \neq 0$ and $v_{\boldsymbol{q}} = 0$.[22,35,36] For singlet pairing, it is expressed as

$$\Gamma_U^{(0)} = \frac{1}{2} \frac{U}{1 + U\chi_0} + \frac{3}{2} \frac{U}{1 - U\chi_0} - U$$
$$= \frac{U}{1 - U^2\chi_0^2} + \frac{U}{1 - U\chi_0} - U, \quad (4.16)$$

which can be written as

$$\Gamma_U^{(0)} = -\frac{1}{4} U^2 \chi_{\mathrm{c}}^{(0)} + 3U^2 \chi_{\mathrm{s}}^{(0)} + U \quad (4.17)$$

with eq. (3.1). For triplet pairing, it is expressed as

$$\Gamma_U^{(0)} = \frac{1}{2} \frac{U}{1 + U\chi_0} + \frac{1}{2} \frac{U}{1 - U\chi_0} = \frac{U}{1 - U^2\chi_0^2}, \quad (4.18)$$

which can be written as

$$\Gamma_U^{(0)} = -\frac{1}{4} U^2 \chi_{\mathrm{c}}^{(0)} + U^2 \chi_{\mathrm{s}}^{(0)} + U. \quad (4.19)$$

In eqs. (4.17) and (4.19), the physical interpretation of each term is clear.[22,35,36] The first terms of eqs. (4.17) and (4.19) are the interactions mediated by the charge fluctuations, while the second terms are those by the spin fluctuations. Obviously, the last constant terms in eqs. (4.17) and (4.19) express the bare on-site Coulomb repulsive interactions, and do not contribute to the gap equation for anisotropic pairing. If we put $v_{\boldsymbol{q}} = 0$, we obtain

$$\Gamma_{\sigma\sigma_1} = \Gamma_U^{(0)}, \quad (4.20)$$

and all the equations are reduced to those in the Hubbard model.

The second term of eq. (4.15) corresponds to the summation of the screened Coulomb and phonon-mediated interactions. If we put $U = 0$, we obtain

$$\Gamma_{\sigma\sigma_1}(q) = \frac{v_{\boldsymbol{q}}}{\kappa_v} \frac{\omega^2}{\omega^2 - [\omega(q)]^2} \equiv \Gamma(q), \quad (4.21)$$

where $\kappa_v = 1 + 2v_{\boldsymbol{q}}\chi_0$ and $\omega(q) = \Omega_{\mathrm{p}}/\sqrt{\kappa_v(q)}$. This equation is easily rewritten as

$$\Gamma_{\sigma\sigma_1}(q) = \frac{v_{\boldsymbol{q}}}{\kappa_v} + [\tilde{M}(q)]^2 \mathcal{D}(q)$$
$$= \frac{v_{\boldsymbol{q}}}{\kappa_v} + \frac{M_{\boldsymbol{q}}^2}{\kappa_v^2} \frac{2\Omega_{\mathrm{p}}}{\omega^2 - [\omega(q)]^2}. \quad (4.22)$$

We note that the expression of $\Gamma_{\sigma\sigma_1}$ in the presence of both U and $v_{\boldsymbol{q}}$, *i.e.*, eq. (4.15), is not obtained by simply adding eqs. (4.20) and (4.21). The second term of eq. (4.15) includes the corrections due to U in a rather complicated manner as explained in the next subsection.

4.4   Interpretation of the corrections due to U

Now, let us interpret how the corrections from U enters in the phonon-mediated pairing interaction, *i.e.*, the second term of eq. (4.15). We can derive eq. (4.15) in another manner as follows, starting from eq. (4.22), *i.e.*, the effective interaction in the absence of U.

First, we rewrite eq. (4.22) as

$$\Gamma_{\sigma\sigma_1}(q) = \frac{v_{\boldsymbol{q}}}{\kappa_v} + \frac{2M_{\boldsymbol{q}}^2}{\kappa_v \Omega_{\mathrm{p}}} \frac{[\omega(q)]^2}{\omega^2 - [\omega(q)]^2}, \quad (4.23)$$

and in this equation we replace κ_v with $\tilde{\kappa}_v$ renormalized by the Hubbard-type charge fluctuations as shown in eq. (3.17). At the same time, we replace the phonon frequency $\omega(q)$ with $\tilde{\omega}(q)$ of the fully dressed phonons, which is given by eq. (3.27). Secondly, we modify the electron-phonon coupling constant $M_{\boldsymbol{q}}$ with

$$\frac{M_{\boldsymbol{q}}}{\kappa_U} = M_{\boldsymbol{q}} \left[1 - U\chi_0 + U^2\chi_0^2 \mp \cdots \right].$$

The series in the right-hand-side is easily verified from the diagramatical technique. At the same time, we insert $1/\kappa_U$ into the both end of the screened Coulomb line which corresponds to $v_{\boldsymbol{q}}/\tilde{\kappa}_v(q)$. In other words, we replace $v_{\boldsymbol{q}}/\tilde{\kappa}_v$ with $v_{\boldsymbol{q}}/\tilde{\kappa}_v\kappa_U^2$. Thirdly, we add the Hubbard-type fluctuation diagrams $\Gamma_U^{(0)}$ including bare U. Then, we obtain the expression of $\Gamma_{\sigma\sigma_1}(q)$

$$\Gamma_{\sigma\sigma_1}(q) = \Gamma_U^{(0)} + \frac{v_{\boldsymbol{q}}}{\kappa_U^2 \tilde{\kappa}_v} + \frac{2M_{\boldsymbol{q}}^2}{\kappa_U^2 \kappa_v \Omega_{\mathrm{p}}} \frac{[\tilde{\omega}(q)]^2}{\omega^2 - [\tilde{\omega}(q)]^2}, \quad (4.24)$$

which coincides with eq. (4.15), since

$$\frac{v_{\boldsymbol{q}}}{\kappa \kappa_U} = \frac{1}{\kappa_U^2} \frac{v_{\boldsymbol{q}}}{\tilde{\kappa}_v} = \frac{2M_{\boldsymbol{q}}^2}{\kappa_U^2 \tilde{\kappa}_v \Omega_{\mathrm{p}}} \quad (4.25)$$

holds from eqs. (3.16) and (2.5).

5.   Effective Interactions for Weak Coupling

In this section, we derive the effective pairing interactions along the scheme of the traditional weak coupling theory. The effective interactions derived here are not suitable for accurate estimations for the transition temperature, but useful for qualitative and semi-quantitative arguments. For quantitative purpose, direct numerical calculations based on the effective vertex eqs. (4.12) and (4.13) is more suitable.

5.1 The case of $U = 0$

First, we briefly review the standard derivation of the effective pairing interactions for $U = 0$.[1] In this case, the total two-particle vertex part $\Gamma_{\sigma\sigma_1}$ is given by eq. (4.21). In this equation, it is explicitly shown that the phonon-mediated interaction is attractive for small ω overcoming repulsive Coulomb interactions. This effect is called the overscreening effect.

In the weak coupling theory, the frequency dependence of the two-particle vertex part $\Gamma(q)$ is simplified by a replacement with a step function as shown in Fig. 8, that is,

$$\Gamma(\boldsymbol{q}, \omega) \approx \frac{v_{\boldsymbol{q}}}{\kappa(\boldsymbol{q}, 0)} \left[1 - \bar{\alpha}\, \theta(\omega_{\mathrm{c}} - |\omega|)\right], \qquad (5.1)$$

where ω_{c} and $\bar{\alpha}$ denote effective constants which express the frequency range and the depth of the attractive part of the interactions. Here, the static approximation for the dielectric function has been introduced.

The effective constants $\bar{\alpha}$ and ω_{c} are complicated quantities that reflect the dispersion energy and the density of states of the dressed phonons. However, it is reasonable to consider that the constant ω_{c} is of the order of the Debye frequency ω_{D}, i.e., the upper limit of the dressed (observed) phonon frequency $\tilde{\omega}_{\boldsymbol{q}}$. According to the standard weak coupling theory, we regard those constants as parameters in this paper.

For isotropic superconductors, the prefactor $v_{\boldsymbol{q}}/\kappa(\boldsymbol{q}, 0)$ is often replaced by an effective constant V_0. We should note that V_0 is an averaged quantity of $v_{\boldsymbol{q}}$ and different from the on-site Coulomb interaction U derived in §2.[7, 11]

Further, in the weak coupling theory, the cutoff ω_{c} in ω integral is taken into account by introducing the same cutoff in ξ integral, where ξ denotes the electron energy measured from the Fermi energy. In other words, we replace the cutoff function $\theta(\omega_{\mathrm{c}} - |\omega|)$ with $\theta(\omega_{\mathrm{c}} - |\xi_{\boldsymbol{k}}|)\theta(\omega_{\mathrm{c}} - |\xi_{\boldsymbol{k}'}|)$.

After these simplifications, we could solve the gap equation along the scheme of the standard weak coupling theory. The Coulomb repulsion, i.e., the first term in the braket of eq. (5.1), is taken into account through the effective Coulomb parameter defined by

$$\mu_{V0}^* = \frac{V_0 N(0)}{1 + V_0 N(0) \ln(W_{\mathrm{C}}/\omega_{\mathrm{c}})}, \qquad (5.2)$$

where W_{C} denotes the cutoff energy of the Coulomb interactions, which is of the order of the band width W.[40] The influence of the Coulomb repulsion is weaken ($\mu_{V0}^* < V_0 N(0)$) by the retardation of the phonon propagation when $\omega_{\mathrm{c}} < W_{\mathrm{C}}$. The superconducting transition temperature T_{c} is given by

$$T_{\mathrm{c}} = 1.13\,\omega_{\mathrm{c}} \mathrm{e}^{-1/(\lambda - \mu_{V0}^*)}, \qquad (5.3)$$

where $\lambda = \bar{\alpha} V_0 N(0)$.
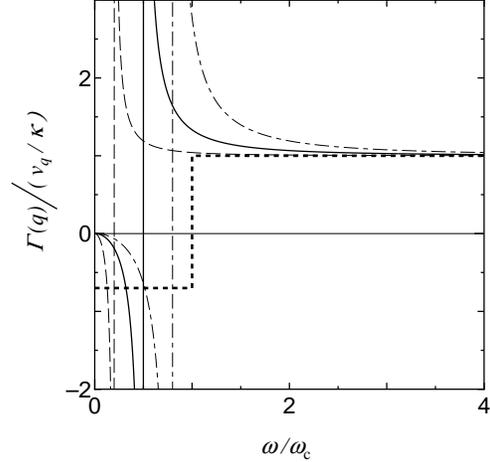
Fig. 8. Schematic figure of the two-particle vertex part $\Gamma(q)$ as a function of $\omega/\omega_{\mathrm{c}}$. The solid, dashed, dot-dashed lines show $\Gamma(q)$ as functions of ω with different fixed values of q. The thick dotted line shows a step function which is introduced to approximate $\Gamma(q)$ in eq. (5.1).

5.2 The case of $U \neq 0$

We extend the above formulation to the case of $U \neq 0$. We introduce the same simplification as eq. (5.1) in the context of the weak coupling theory. Hence, it is obtained that

$$\Gamma_{\sigma\sigma_1}(\boldsymbol{q}, \omega) = \Gamma_U^{(0)} + \tilde{v}_{\boldsymbol{q}} \left[1 - \bar{\alpha}\, \theta(\omega_{\mathrm{c}} - |\omega|)\right], \qquad (5.4)$$

with $\tilde{v}_{\boldsymbol{q}} \equiv v_{\boldsymbol{q}}/\kappa(\boldsymbol{q}, 0)\kappa_U(\boldsymbol{q}, 0)$, where the static approximation has been also introduced in κ, κ_U and $\Gamma_U^{(0)}$ as in eq. (5.1).

Let us compare the expressions for $U = 0$ and $U \neq 0$, i.e., eqs. (5.1) and (5.4). One of the important differences is that eq. (5.4) includes the Hubbard-type effective interaction $\Gamma_U^{(0)}$ that we have discussed in §4.3.

Another difference between eqs. (5.1) and (5.4) is the renormalization of the second term of eq. (5.4) due to the on-site Coulomb interaction U. In this term, the prefactor $\tilde{v}_{\boldsymbol{q}}$ and the constants $\bar{\alpha}$ and ω_{c} are modified. The constants $\bar{\alpha}$ and ω_{c} are usually treated as parameters in the weak coupling theory, and sometimes determined by experiments. Hence, we do not need to know the differences from their original values, and the modifications in $\bar{\alpha}$ and ω_{c} do not need to be considered explicitly. Therefore, the important modification is in the prefactor $\tilde{v}_{\boldsymbol{q}}$, because it affects the momentum dependence. From eqs. (3.16) and (3.17), it is written as

$$\tilde{v}_{\boldsymbol{q}} \equiv \frac{v_{\boldsymbol{q}}}{\kappa \kappa_U} = \frac{1}{2\chi_0 \kappa_U} \frac{\tilde{q}_s^2}{|\boldsymbol{q}|^2 + \tilde{q}_s^2}. \qquad (5.5)$$

Putting $U = 0$ in eq. (5.5), it reduces to the factor of

eq. (5.1), *i.e.*,

$$\frac{1}{2\chi_0}\frac{q_s^2}{|\boldsymbol{q}|^2 + q_s^2}. \tag{5.6}$$

Comparing eqs. (5.5) and (5.6), we note that q_s is replaced with a smaller quantity $\tilde{q}_s$ in eq. (5.5). As discussed in §3.2, the screening length $\lambda_{\rm scr} = q_{\rm TF}^{-1} = [q_s]_{q=0}^{-1}$ is lengthened into $\tilde{\lambda}_{\rm scr} = [\tilde{q}_s]_{q=0}^{-1}$ because $U > 0$. Then, the peak of eq. (5.5) becomes sharper, and the anisotropic components increase.

In summary of this part, we find two effects of the short-range correlations: (1) The Hubbard term $\Gamma_U^{(0)}$, which includes bare U, is added as pointed out in the previous section §4; (2) The short-range correlations change the momentum dependence of the phonon-mediated pairing interaction. Both effects unfavor isotropic pairing, but favor anisotropic pairing of some symmetries.

It is also found that for this mechanism of triplet pairing, the existence of the on-site Coulomb interaction U is essential, but not the s-wave (isotropic) component of $v_{\boldsymbol{q}}$, such as V_0. We note in the second term of eq. (5.4) that the long-range part $\tilde{v}_{\boldsymbol{q}}$ of the Coulomb interaction and the phonon-mediated pairing interaction $-\alpha\tilde{v}_{\boldsymbol{q}}\theta(\omega_{\rm c}-|\omega|)$ have the same momentum dependence. Hence, it is not effective for the change in the dominancy of the coupling constants. In fact, when we put the dominant isotropic component V_0 and the subdominant anisotropic component V_1, the difference of the effective coupling constants which include the negative contributions of the effective Coulomb parameters is calculated as

$$\begin{aligned}
&\left[\bar{\alpha}V_0 - \frac{V_0}{1 + V_0 x}\right] - \left[\bar{\alpha}V_1 - \frac{V_1}{1 + V_1 x}\right] \\
&= (V_0 - V_1)\left[\bar{\alpha} - \frac{1}{(1 + V_0 x)(1 + V_1 x)}\right],
\end{aligned} \tag{5.7}$$

where $x \equiv N(0)\ln(W_{\rm C}/\omega_{\rm c})$. We have $\bar{\alpha} > 1$ when the overscreening effect gives rise to a net attractive interaction for low frequencies. Thus, when $V_0 > V_1$, the right-hand-side of eq. (5.7) is positive. Therefore, it is found that the long-range part $\tilde{v}_{\boldsymbol{q}}$, which gives rise to the third and fourth terms in the left-hand-side of eq. (5.7), does not change the sign of eq. (5.7). In the rest of this paper, we investigate the change in the dominancy of the coupling constants due to the Coulomb interaction more explicitly.

5.3 Interactions mediated by spin fluctuations

In this subsection, we develop a weak coupling theory including interactions mediated by spin fluctuations through $\Gamma_U^{(0)}$. In particular, when the spin fluctuations are relevant, the vertex part $\Gamma_U^{(0)}(\boldsymbol{q},\omega)$ consists of two parts as a function of $\boldsymbol{q}$ and ω: (a) A broad peak that reflects the energy scale of the band width $\sim W$; (b) A sharp peak that reflects the energy scale of the spin fluctuations $\omega_{\rm sf}$, as discussed in our previous papers.[17,22]

Hence, we write it in the form

$$\Gamma_U^{(0)}(\boldsymbol{q},\omega) \approx \bar{\Gamma}_U^{(0)}(\boldsymbol{q},0) + \Gamma_{\rm sf}^{(0)}(\boldsymbol{q},0)\theta(\omega_{\rm sf} - |\omega|), \tag{5.8}$$

where the first and second terms which correspond to (a) and (b) mentioned above, respectively. Obviously, $\bar{\Gamma}_U^{(0)}$ includes the on-site Coulomb repulsive interaction. Therefore, we obtain

$$\begin{aligned}
\Gamma_{\sigma\sigma_1}(\boldsymbol{q},\omega) &= V_{\rm C}(\boldsymbol{q}) + \Gamma_{\rm sf}^{(0)}(\boldsymbol{q},0)\theta(\omega_{\rm sf} - |\omega|) \\
&\quad - \bar{\alpha}\tilde{v}_{\boldsymbol{q}}\,\theta(\omega_{\rm c} - |\omega|)
\end{aligned} \tag{5.9}$$

from eq. (5.4), where we have defined a Coulomb term $V_{\rm C}(\boldsymbol{q}) \equiv \bar{\Gamma}_U^{(0)}(\boldsymbol{q},0) + \tilde{v}_{\boldsymbol{q}}$.

As mentioned in §5.1, we replace $\theta(\omega_k - |\omega|)$ with $\theta(\omega_k - |\xi_{\boldsymbol{k}}|)\theta(\omega_k - |\xi_{\boldsymbol{k}'}|)$ within the weak coupling theory, where $\omega_1 = \omega_{\rm c}$ and $\omega_2 = \omega_{\rm sf}$. Therefore, we obtain effective interactions

$$V_{\rm eff}(\boldsymbol{k},\boldsymbol{k}') = V_{\rm C}(\boldsymbol{k} - \boldsymbol{k}') + V_{\rm sf}(\boldsymbol{k},\boldsymbol{k}') + V_{\rm ph}(\boldsymbol{k},\boldsymbol{k}'), \tag{5.10}$$

where

$$\begin{aligned}
V_{\rm sf}(\boldsymbol{k},\boldsymbol{k}') &= \Gamma_{\rm sf}^{(0)}(\boldsymbol{k} - \boldsymbol{k}',0)\theta(\omega_{\rm sf} - |\xi_{\boldsymbol{k}}|)\theta(\omega_{\rm sf} - |\xi_{\boldsymbol{k}'}|) \\
V_{\rm ph}(\boldsymbol{k},\boldsymbol{k}') &= -\bar{\alpha}\tilde{v}_{\boldsymbol{k}-\boldsymbol{k}'}\theta(\omega_{\rm c} - |\xi_{\boldsymbol{k}}|)\theta(\omega_{\rm c} - |\xi_{\boldsymbol{k}'}|).
\end{aligned} \tag{5.11}$$

When $\omega_{\rm sf} \ll W$ and $\omega_{\rm c} \ll W$, we may regard $\Gamma_{\rm sf}^{(0)}$ and $\tilde{v}_{\boldsymbol{k}-\boldsymbol{k}'}$ as functions of $k_\parallel$ and $k'_\parallel$, which denote the momentum components of $\boldsymbol{k}$ and $\boldsymbol{k}'$ along the Fermi surface. Hence, we introduce a complete set of the basis functions $\gamma_\alpha(k_\parallel)$ with $\alpha = 0, 1, 2, \cdots$, which are normalized by the average on the Fermi surface. For example, we may replace $k_\parallel$ with $\hat{\boldsymbol{k}} \equiv \boldsymbol{k}/|\boldsymbol{k}|$ or (θ,φ), and take $\alpha = s, p_x, p_y, p_x \cdots$ or $\alpha = (l,m)$ in the spherically symmetric systems. We define $V_{\rm sf}(k_\parallel, k'_\parallel) \equiv [\Gamma_{\rm sf}^{(0)}(\boldsymbol{k} - \boldsymbol{k}',0)]_{\xi_{\boldsymbol{k}}=\xi'_{\boldsymbol{k}}=0}$ and $V_{\rm ph}(k_\parallel, k'_\parallel) \equiv -\bar{\alpha}[\tilde{v}_{\boldsymbol{k}-\boldsymbol{k}'}]_{\xi_{\boldsymbol{k}}=\xi'_{\boldsymbol{k}}=0}$, and expand the interactions as

$$V_k(k_\parallel, k'_\parallel) = \sum_\alpha V_k^\alpha \gamma_\alpha(k_\parallel)\gamma_\alpha(k'_\parallel), \tag{5.12}$$

where the index k donotes the kind of interactions, for example, $V_1 = V_{\rm ph}$, $V_2 = V_{\rm sf}$ and $V_3 = V_{\rm C}$. We define dimensionless coupling constants $\lambda_{\rm ph}^\alpha = -V_{\rm ph}^\alpha N(0)$ and $\lambda_{\rm sf}^\alpha = -V_{\rm sf}^\alpha N(0)$, and effective Coulomb parameter $\mu_\alpha^* = V_{\rm C}^\alpha N(0)/[1 + V_{\rm C}^\alpha N(0)\ln(W_{\rm C}/\omega_{\rm c})]$.

The gap function is also expanded as

$$\Delta(\boldsymbol{k}) = \sum_\alpha \Delta_\alpha \gamma_\alpha(k_\parallel) \tag{5.13}$$

on the Fermi surface. By taking the basis functions γ_α appropriately, we can make the gap equation diagonal with respect to the symmetry index α upto the linear order of Δ. While each decoupled gap equation gives a different second order transition temperature $T_{c\alpha}$, we must take the highest one of $T_{c\alpha}$'s, since the system exhibits superconductivity when at least one of Δ_α's is nonzero.

In the same way as in our previous paper,[17] we can obtain the transition temperature $T_{\rm c}$ and the isotope effect

coefficient α_{IE} defined by

$$\alpha_{\mathrm{IE}} = -\frac{\partial \ln T_{\mathrm{c}}}{\partial \ln M}, \qquad (5.14)$$

where M denotes the relevant atomic mass. Because the application is straightforward, we shall omit the derivation and only present the results.

When $\omega_{\mathrm{sf}} < \omega_{\mathrm{c}} \sim \omega_{\mathrm{D}}$, which occurs in the proximity of the magnetic instability, we obtain the transition temperature $T_{\mathrm{c}} = 1.13\,\omega_{\mathrm{c}} \exp[-1/(\lambda_{\mathrm{sf}}^{\alpha} + \lambda_{\mathrm{ph}}^{\alpha*})]$ with $\lambda_{\mathrm{ph}}^{\alpha*} = (\lambda_{\mathrm{ph}}^{\alpha} - \mu_{\alpha}^{*})/[1 - (\lambda_{\mathrm{ph}}^{\alpha} - \mu_{\alpha}^{*}) \ln(\omega_{\mathrm{c}}/\omega_{\mathrm{sf}})]$ and the isotope effect coefficient

$$\alpha_{\mathrm{IE}} = \frac{1}{2}\Big(\frac{\lambda_{\mathrm{ph}}^{\alpha*}}{\lambda_{\mathrm{sf}}^{\alpha} + \lambda_{\mathrm{ph}}^{\alpha*}}\Big)^2 \Big[1 - \Big(\frac{\mu_{\alpha}^{*}}{\lambda_{\mathrm{ph}}^{\alpha} - \mu_{\alpha}^{*}}\Big)^2\Big]. \qquad (5.15)$$

When $\omega_{\mathrm{sf}} > \omega_{\mathrm{c}} \sim \omega_{\mathrm{D}}$, which occurs away from the magnetic instability, we obtain the transition temperature $T_{\mathrm{c}} = 1.13\,\omega_{\mathrm{c}} \exp[-1/(\lambda_{\mathrm{ph}}^{\alpha} + \lambda_{\mathrm{sf}}^{\alpha*})]$ with $\lambda_{\mathrm{sf}}^{\alpha*} = (\lambda_{\mathrm{sf}}^{\alpha} - \mu_{\mathrm{sf}}^{\alpha*})/[1 - (\lambda_{\mathrm{sf}}^{\alpha} - \mu_{\mathrm{sf}}^{\alpha*}) \ln(\omega_{\mathrm{sf}}/\omega_{\mathrm{c}})]$ and $\mu_{\mathrm{sf}}^{\alpha*} = V_{\mathrm{C}}^{\alpha} N(0)/[1 + V_{\mathrm{C}}^{\alpha} N(0) \ln(W_{\mathrm{C}}/\omega_{\mathrm{sf}})]$. The isotope effect coefficient is obtained as

$$\alpha_{\mathrm{IE}} = \frac{1}{2}\Big[1 - \Big(\frac{\lambda_{\mathrm{sf}}^{\alpha*}}{\lambda_{\mathrm{ph}}^{\alpha} + \lambda_{\mathrm{sf}}^{\alpha*}}\Big)^2\Big]. \qquad (5.16)$$

5.4 Anisotropic pairing mediated by phonons

In this subsection, we derive expressions of the effective coupling constants and the effective Coulomb parameters for anisotropic pairing. We concentrate our attention on the interactions mediated by phonons, and ignore the attractive interactions by $\Gamma_U^{(0)}$.

Hence, we consider the case in which we could ignore the momentum and frequency dependences of $\chi_0(q)$, so that $\chi_0(q) \approx \chi_0(\mathbf{0}, 0) = N(0)$ holds. Although this simplification becomes qualitatively better away from the magnetic instability, even there the spin fluctuations still have an important effect of enhancement of the repulsive Coulomb interactions as

$$\frac{U}{1 - U\chi_0(0)} = U + U^2 \chi_{\mathrm{s}}^{(0)}(0) > U. \qquad (5.17)$$

Further, since $\Gamma_U^{(0)}$ becomes constant in the simplification mentioned above, it affects only s-wave pairing. Hence, we use the expression of $\Gamma_U^{(0)}$ for singlet pairing eq. (4.16). From eqs. (5.4) and (5.5), we obtain

$$\Gamma_{\sigma\sigma'}(\mathbf{q}, \omega) N(0) = \frac{\mu_{\mathrm{C}}}{1 - \mu_{\mathrm{C}}^2} + \frac{\mu_{\mathrm{C}}^2}{1 - \mu_{\mathrm{C}}} + \frac{\tilde{F}(\mathbf{q})}{2(1 + \mu_{\mathrm{C}})}$$
$$- \frac{gN(0)}{1 + \mu_{\mathrm{C}}} \tilde{F}(\mathbf{q})\, \theta(\omega_{\mathrm{c}} - |\omega|), \qquad (5.18)$$

where we have defined a parameter g by $\bar{\alpha} = 2gN(0)$ and

$$\tilde{F}(\mathbf{q}) \equiv \frac{\tilde{q}_s^2}{|\mathbf{q}|^2 + \tilde{q}_s^2} \qquad (5.19)$$

with

$$\tilde{q}_s^2 = \frac{q_s^2}{1 + \mu_{\mathrm{C}}} = \frac{q_{\mathrm{TF}}^2}{1 + \mu_{\mathrm{C}}}. \qquad (5.20)$$

We expand $\tilde{F}(\mathbf{q})$ and $\Delta(\mathbf{k})$ on the Fermi surface with respect to the momentum components parallel to the Fermi surface as in eqs. (5.12) and (5.13). We define the expansion factors C_{α} of $\tilde{F}$ by

$$\tilde{F}(\mathbf{k} - \mathbf{k}') = \sum_{\alpha} C_{\alpha} \gamma_{\alpha}(k_{\parallel}) \gamma_{\alpha}(k_{\parallel}'). \qquad (5.21)$$

For convenience, we write $\alpha = 0$ for s-wave pairing, while $\alpha \neq 0$ for anisotropic pairing, from now on.

Therefore, from eq. (5.18) and the replacement of $\theta(\omega_{\mathrm{c}} - |\omega|)$ with $\theta(\omega_{\mathrm{c}} - |\xi_{\mathbf{k}}|)\theta(\omega_{\mathrm{c}} - |\xi_{\mathbf{k}'}|)$ that is adopted in §5.1 and §5.3, the α component of the effective interactions is written in the form

$$V_{\alpha} N(0) = -\lambda_{\alpha}\theta(\omega_{\mathrm{c}} - |\xi_{\mathbf{k}}|)\theta(\omega_{\mathrm{c}} - |\xi_{\mathbf{k}'}|) + \mu_{\alpha}, \quad (5.22)$$

where λ_{α} and μ_{α} denote the dimensionless coupling constants of the phonon-mediated pairing interaction and the repulsive Coulomb interaction, for "α-wave" superconductivity, which are expressed as follows. The constant λ_{α} is expressed as

$$\lambda_{\alpha} = \frac{gN(0)}{1 + \mu_{\mathrm{C}}} C_{\alpha}, \qquad (5.23)$$

for any value of α. In contrast, the constant μ_{α} has different forms depending on $\alpha = 0$ or $\alpha \neq 0$. For s-wave pairing ($\alpha = 0$), we obtain

$$\mu_0 = \frac{\mu_{\mathrm{C}}}{1 - \mu_{\mathrm{C}}^2} + \frac{\mu_{\mathrm{C}}^2}{1 - \mu_{\mathrm{C}}} + \frac{C_0}{2(1 + \mu_{\mathrm{C}})}, \qquad (5.24)$$

while for anisotropic "α-wave" pairing ($\alpha \neq 0$)

$$\mu_{\alpha} = \frac{C_{\alpha}}{2(1 + \mu_{\mathrm{C}})}. \qquad (5.25)$$

For the retardation effect, the effective Coulomb parameter μ_{α}^{*} becomes smaller than μ_{α} as

$$\mu_{\alpha}^{*} = \frac{\mu_{\alpha}}{1 + \mu_{\alpha} \ln(W_{\mathrm{C}}/\omega_{\mathrm{c}})}. \qquad (5.26)$$

The derivation of eq. (5.26) is explained, for example, in Refs. 1 and 17. The superconducting transition temperature for "α-wave" pairing is estimated from the above parameters by the equation

$$T_{\mathrm{c}\alpha} = 1.13\,\omega_{\mathrm{c}}\mathrm{e}^{-1/\tilde{\lambda}_{\alpha}}, \qquad (5.27)$$

where $\tilde{\lambda}_{\alpha} = \lambda_{\alpha} - \mu_{\alpha}^{*}$. As argued below eq. (5.13), the real transition temperature T_{c} is the highest one among all $T_{\mathrm{c}\alpha}$'s.

We obtain the isotope effect coefficient

$$\alpha_{\mathrm{IE}} = \frac{1}{2}\left[1 - \Big(\frac{\mu_{\alpha}^{*}}{\tilde{\lambda}_{\alpha}}\Big)^2\right], \qquad (5.28)$$

putting $\lambda_{\mathrm{sf}}^{\alpha} = 0$ in eq. (5.15). The reverse isotope effect $\alpha_{\mathrm{IE}} < 0$ occurs when $\mu_{\alpha}^{*} > \tilde{\lambda}_{\alpha}$, i.e., $2 > \lambda_{\alpha}/\mu_{\alpha}^{*}$.

From eqs. (5.23) and (5.25), we have $\lambda_\alpha/\mu_\alpha = 2gN(0)$ for anisotropic pairing. Hence, for $\alpha_{\mathrm{IE}} < 0$ to occur in anisotropic superconductors, the inequality $1 > gN(0)$ needs to hold, because $2 > \lambda_\alpha/\mu_\alpha^* > \lambda_\alpha/\mu_\alpha > 2gN(0)$. However, for such weak coupling, the transition temperature becomes extremely low so that it is not practically observable. If we take into account repulsive contribution to μ_α from $\Gamma_U^{(0)}$, which modifies eq. (5.25), the reverse isotope effect $\alpha_{\mathrm{IE}} < 0$ is possible even in the present situation.[17]

In eq. (5.26), the Coulomb cutoff energy W_{C} is usually of the order of the band width W. More precisely, it is defined by

$$\ln W_{\mathrm{C}} \equiv \frac{1}{2}\left[\ln\left(W - \epsilon_{\mathrm{F}}\right) + \ln \epsilon_{\mathrm{F}}\right] \qquad (5.29)$$

as is easily verified from the derivation of eq. (5.26), where W and ϵ_{F} denote the band width and the chemical potential (Fermi energy) measured from the bottom of the electron band. Equation (5.29) is written as $W_{\mathrm{C}} = \sqrt{\epsilon_{\mathrm{F}}(W - \epsilon_{\mathrm{F}})}$. Hence, it is easily proved that $W_{\mathrm{C}} \leq W/2$, where the equal sign holds when $\epsilon_{\mathrm{F}} = W/2$. In particular, when the charge carrier density is very small as in semi-metals, that is, $\epsilon_{\mathrm{F}} \ll W$, we obtain $W_{\mathrm{C}} \approx \sqrt{W \epsilon_{\mathrm{F}}} \ll W$.

5.5 Dimensionality and anisotropic pairing

As we could see in eqs. (5.18) - (5.21), the anisotropic pairing interactions can dominate when $\tilde{q}_{\mathrm{s}}$ is small and $C_{\alpha \neq 0}$ is near C_0. Since $\tilde{q}_{\mathrm{s}}$ is proportional to q_{TF} as seen in eq. (5.20), small q_{TF} favors anisotropic pairing. In systems with isotropic Fermi surfaces, we have

$$\tilde{F}(\boldsymbol{q}) = \frac{\tilde{q}_{\mathrm{s}}^2/2k_{\mathrm{F}}^2}{1 - \cos\theta + \tilde{q}_{\mathrm{s}}^2/2k_{\mathrm{F}}^2} = \frac{\alpha_{\mathrm{s}} - 1}{\alpha_{\mathrm{s}} - \cos\theta}, \qquad (5.30)$$

where $\alpha_{\mathrm{s}} = 1 + \tilde{q}_{\mathrm{s}}^2/2k_{\mathrm{F}}^2 = 1 + q_{\mathrm{TF}}^2/2k_{\mathrm{F}}^2(1 + \mu_{\mathrm{C}})$, and θ denotes the angle between $\boldsymbol{k}$ and $\boldsymbol{k}'$, since $\boldsymbol{q} = \boldsymbol{k} - \boldsymbol{k}'$. Thus, it is found that the scaled parameters $q_{\mathrm{TF}}^2/2k_{\mathrm{F}}^2$ and μ_{C} are the essential parameters in the sense that they determine the property of the function $\tilde{F}(\boldsymbol{q})$.

First, we discuss the three dimensional system. In systems with spherically symmetric Fermi surfaces,[7] we obtain

$$\frac{q_{\mathrm{TF}}^2}{2k_{\mathrm{F}}^2} = \frac{2}{\pi(3\pi^2)^{1/3}n^{1/3}} \frac{m_{\mathrm{b}}}{m} \frac{a}{a_{\mathrm{B}}} \approx \frac{1}{n^{1/3}} \frac{m_{\mathrm{b}}}{m} \frac{a}{2.6[\text{Å}]} \quad (5.31)$$

where m, m_{b}, a_{B} and n denote the bare electron mass, the band effective mass, the Borh radius $a_{\mathrm{B}} = \hbar^2/me^2 \approx 0.5293\text{Å}$, and the electron (or charge carrier of $\pm e$) density per a site, respectively. Therefore, as the lattice constant a increases, the ratio $q_{\mathrm{TF}}^2/2k_{\mathrm{F}}^2$ increases, which implies stronger screening.

We obtain a qualitatively different result in the quasi-two-dimensional system. In systems with cylindrically symmetric Fermi surfaces,[11] we obtain

$$\frac{q_{\mathrm{TF}}^2}{2k_{\mathrm{F}}^2} = \frac{1}{\pi n} \frac{m_{\mathrm{b}}}{m} \frac{a^2}{a_{\mathrm{B}} d} \approx \frac{1}{n} \frac{m_{\mathrm{b}}}{m} \frac{a^2}{1.7[\text{Å}] \times d}, \qquad (5.32)$$

where a and d denote the lattice constant in the layer and the layer interval. As pointed out in our previous paper,[11] as the layer interval d increases, the ratio $q_{\mathrm{TF}}^2/2k_{\mathrm{F}}^2$ decreases, which implies weaker screening, in contrast to the result in the three-dimensional systems mentioned above.

6.   Examples of the Application

Purpose of this section is to show examples of the application of the effective Hamiltonian derived in the previous section. For simplicity, we consider spherical symmetric systems. We have already examined a spherical symmetric system in our previous paper,[7] but the present treatment is based on a more basic model. Consequently, the corrections due to U are taken into account in more detail. The transition temperatures obtained in this section should be taken as crude estimations, because the model is simplified. Nevertheless, the qualitative results obtained here reflect essential aspects of the present mechanism.

From the symmetry, we take the basis function as $\gamma_\alpha(\hat{\boldsymbol{k}}) = Y_{lm}(\theta, \varphi)$ with $\alpha = (l, m)$. Therefore,

$$\tilde{F}(\boldsymbol{k} - \boldsymbol{k}') = \sum_{l,m} C_l \left[Y_{lm}(\theta, \varphi)\right]^* Y_{lm}(\theta', \varphi')$$

$$= \sum_l (2l + 1) C_l P_l(\cos\theta_{\boldsymbol{k}\boldsymbol{k}'}) \qquad (6.1)$$

$$\Delta(\hat{\boldsymbol{k}}) = \sum_{lm} \Delta_{lm} Y_{lm}(\theta, \varphi),$$

where $\theta_{\boldsymbol{k}\boldsymbol{k}'}$ denotes the angle between $\boldsymbol{k}$ and $\boldsymbol{k}'$. Since $P_0(w) = 1$ and $P_1(w) = w$, we obtain from eq. (5.30)

$$C_0 = \int \frac{\mathrm{d}\Omega}{4\pi} \frac{\alpha_{\mathrm{s}} - 1}{\alpha_{\mathrm{s}} - \cos\theta} = -\frac{\alpha_{\mathrm{s}} - 1}{2} \ln\left|\frac{\alpha_{\mathrm{s}} - 1}{\alpha_{\mathrm{s}} + 1}\right|$$

$$C_1 = \int \frac{\mathrm{d}\Omega}{4\pi} \frac{(\alpha_{\mathrm{s}} - 1)\cos\theta}{\alpha_{\mathrm{s}} - \cos\theta} \qquad (6.2)$$

$$= -(\alpha_{\mathrm{s}} - 1)\left[1 + \frac{\alpha_{\mathrm{s}}}{2} \ln\left|\frac{\alpha_{\mathrm{s}} - 1}{\alpha_{\mathrm{s}} + 1}\right|\right],$$

where $\mathrm{d}\Omega = \sin\theta \, \mathrm{d}\theta \, \mathrm{d}\varphi$. Considering the signs of the three quantity, $\tilde{\lambda}_0$, $\tilde{\lambda}_1$, and $\tilde{\lambda}_0 - \tilde{\lambda}_1$, we obtain the phase diagrams as shown in the following subsections.

6.1 Typical parameter values for ordinary metals

Figure 9 shows the phase diagram for the set of parameter values $W_{\mathrm{C}}/\omega_{\mathrm{c}} = 100$ and $q_{\mathrm{TF}}^2/2k_{\mathrm{F}}^2 = 0.5$. The formar ratio $W_{\mathrm{C}}/\omega_{\mathrm{c}} = 100$ is typical of most metallic systems since $W_{\mathrm{C}} \sim W$ and $\omega_{\mathrm{c}} \sim \omega_{\mathrm{D}}$. The latter ratio $q_{\mathrm{TF}}^2/2k_{\mathrm{F}}^2 = 0.5$ implies the Thomas-Fermi screening length $\lambda_{\mathrm{TF}} = 1/k_{\mathrm{F}} \sim a/\pi$, which seems typical of metals, too. Because at $\mu_{\mathrm{C}} = U_{\mathrm{c}}N(0) \approx 1$, the magnetic instability $\chi_{\mathrm{s}} \to \infty$ should occur, the results are plotted only for $UN(0) < 1$. It is found that the triplet state occurs for large U, which confirms one of our previous results.[7] It is also found that for large g, the s-wave state is more favored than the p-wave state.
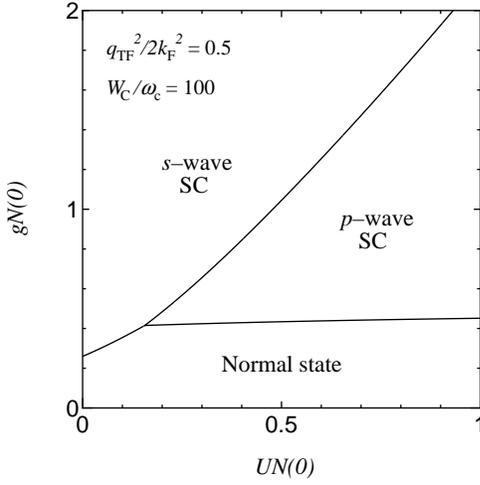
Fig. 9. The phase diagram on the plane of the on-site Coulomb energy U and the effective coupling constant g of the phonon-mediated pairing interaction, in the spherical symmetric system. The parameters are chosen as $q_{\mathrm{TF}}^2/2k_{\mathrm{F}}^2 = 0.5$ and $W_{\mathrm{C}}/\omega_{\mathrm{c}} = 100$. The abbreviation SC stands for superconductivity.

Fig. 11. The transition temperatures as functions of the effective constant g of the phonon-mediated interaction for the narrow band case, in which we set $q_{\mathrm{TF}}^2/2k_{\mathrm{F}}^2 = 0.5$, $W_{\mathrm{C}}/\omega_{\mathrm{c}} = 5$. We have put $\omega_{\mathrm{c}} = 300$ K as an example. The solid and dashed lines show the transition temperatures $T_{\mathrm{c}p}$ and $T_{\mathrm{c}s}$ of the p-wave and s-wave states for $UN(0) = 0.5$. For each value of $gN(0)$, the higher one of $T_{\mathrm{c}p}$ and $T_{\mathrm{c}s}$ is the final result of T_{c}, $i.e.$, the physical T_{c}. The thin solid and dashed lines show those for $UN(0) = 0.7$.

Fig. 10. The phase diagram for a narrow band case, in which we set $q_{\mathrm{TF}}^2/2k_{\mathrm{F}}^2 = 0.5$ and $W_{\mathrm{C}}/\omega_{\mathrm{c}} = 5$. Along the vertical thin dotted line, the transition temperatures are plotted in Fig. 11.
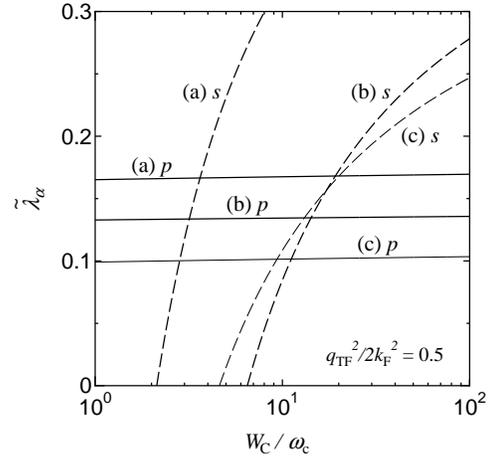
Fig. 12. The dimensionless coupling constants $\tilde{\lambda}_\alpha$ as functions of $W_{\mathrm{C}}/\omega_{\mathrm{c}}$. The solid and dashed lines denote $\tilde{\lambda}_p$ and $\tilde{\lambda}_s$, respectively. The parameter values are taken as (a) $gN(0) = 3$, $UN(0) = 0.5$, (b) $gN(0) = 3$, $UN(0) = 0.8$, and (c) $gN(0) = 2$, $UN(0) = 0.5$.

Therefore, for the present set of parameter values, the resultant dimensionless coupling constant $\tilde{\lambda}_p$ for the p-wave state is quite small, where it overcomes the s-wave state. For example, when $\mu_{\mathrm{C}} = UN(0) = 0.5$, the highest transition temperature to the p-wave state occurs near the phase boundary at $gN(0) \approx 1.05$. However, at $\mu_{\mathrm{C}} = 0.5$ and $gN(0) = 1.0$, we obtain $\tilde{\lambda}_0 \approx 0.031$ and $\tilde{\lambda}_1 \approx 0.037$, and such a small value of $\tilde{\lambda}_1$ gives $T_{\mathrm{c}p} \sim 10^{-10}$K, which is too low to be observed in practice. For $gN(0) \gtrsim 1.05$, we obtain larger T_{c}, but there

the s-wave state occurs. This result is consistent with the experimental fact that spin-triplet superconductivity has not been observed in the ordinary metals.

6.2 Narrow band systems

Next, we examine systems in which the ratio $W_{\mathrm{C}}/\omega_{\mathrm{c}}$ is not so large. From eq. (5.29), since $W_{\mathrm{C}}/\omega_{\mathrm{c}} \sim$

$\sqrt{\epsilon_{\mathrm{F}}(W - \epsilon_{\mathrm{F}})}/\omega_{\mathrm{D}}$, such a situation is realized, for example, in semi-metals with extremely small ϵ_{F} and in narrow band systems with extremely small W. In such systems, since $\omega_{\mathrm{c}} \ll W$ or $\omega_{\mathrm{c}} \ll \epsilon_{\mathrm{F}}$ does not hold, the approximation $N(\epsilon) \approx N(0)$ is not correct quantitatively, but it is not essential for our purpose. The phase diagram for $q_{\mathrm{TF}}^2/2k_{\mathrm{F}}^2 = 0.5$ and $W_{\mathrm{C}}/\omega_{\mathrm{c}} = 5$ is presented in Fig. 10. Since $W \gtrsim 2W_{\mathrm{C}} = 10\omega_{\mathrm{c}} \sim 10\omega_{\mathrm{D}}$, if we put $\omega_{\mathrm{D}} = 300$ K, we obtain $W \gtrsim 0.3$ eV. As the ratio $W_{\mathrm{C}}/\omega_{\mathrm{c}}$ becomes smaller, since the retardation effect becomes weaker, s-wave pairing is suppressed more effectively by the on-site Coulomb repulsion. As a result, the area for the p-wave state is enlarged in the phase diagram, and $T_{\mathrm{c}p}$ becomes large enough to be observed in contrast to the result in the previous subsection §6.1.

In Fig. 11, the transition temperatures for the parameter values of Fig. 10 are plotted, where we have put $\omega_{\mathrm{D}} = 300$ K as an example. For $UN(0) = 0.5$, it is found that the transition temperature $T_{\mathrm{c}p}$ to the triplet state could reach 0.3 K at $gN(0) \approx 2.6$, while for $gN(0) \gtrsim 2.6$, s-wave superconductivity occurs since $T_{\mathrm{c}s} > T_{\mathrm{c}p}$. In contrast, for $UN(0) = 0.7$, since $T_{\mathrm{c}p} > T_{\mathrm{c}s}$ upto $gN(0) \approx 4$, because s-wave pairing is strongly suppressed by the on-site U. Thus, $T_{\mathrm{c}p}$ could reach a rather larger value 2 K, where the triplet state occurs.

Figure 12 shows the dimensionless coupling constants $\tilde{\lambda}_\alpha$ as functions of $W_{\mathrm{C}}/\omega_{\mathrm{c}}$. It is found that the p-wave state is favored for narrower band widths W ($\sim 2W_{\mathrm{C}}$), because the on-site U suppresses s-wave pairing more effectively. The coupling constants $\tilde{\lambda}_p$ for p-wave pairing depend on $W_{\mathrm{C}}/\omega_{\mathrm{c}}$ slightly. If we put $\omega_{\mathrm{c}} \approx \omega_{\mathrm{D}} = 300$ K, we could estimate $T_{\mathrm{c}p}$ as $T_{\mathrm{c}p} = 0.015$ K, 0.16 K, and 0.79 K, for $\tilde{\lambda}_p = 0.1$, 0.13, and 0.165, respectively. Therefore, for $q_{\mathrm{TF}}^2/2k_{\mathrm{F}}^2 = 0.5$, which gives $\lambda_{\mathrm{TF}} \sim 1/k_{\mathrm{F}} \gtrsim a/\pi \sim 0.3 \times a$, the transition temperature $T_{\mathrm{c}p}$ can be high enough to be observed in practice, where the s-wave state is suppressed by strong on-site Coulomb repulsion. For this mechanism, the smallness of the ratio $W_{\mathrm{C}}/\omega_{\mathrm{c}}$ is essential.

6.3   Systems with weak Coulomb screening

Next, we examine systems with weak Coulomb screening. As examined in our previous paper[11] and briefly discussed in §5.5, the screening can be weak, for example in layered systems with sufficiently large intervals between the layers, although here we examine spherically symmetric systerms.

Now, let us examine the case with $q_{\mathrm{TF}}^2/2k_{\mathrm{F}}^2 = 0.1$ and $W_{\mathrm{C}}/\omega_{\mathrm{c}} = 100$. For $q_{\mathrm{TF}}^2/2k_{\mathrm{F}}^2 = 0.1$, we obtain $\lambda_{\mathrm{TF}} = \sqrt{5}/k_{\mathrm{F}} \gtrsim \sqrt{5}a/\pi \sim 0.7 \times a$. The short-range correlations lengthen the screening length by $\sqrt{1 + \mu_{\mathrm{C}}}$ as shown in eq. (3.18). In Fig. 13, the area of the p-wave state is much larger than those in Figs. 9 and 10. Thus, we confirm that as the screening becomes weaker, the anisotropic pairing interactions increase, as proposed in our previous papers.[7,11]
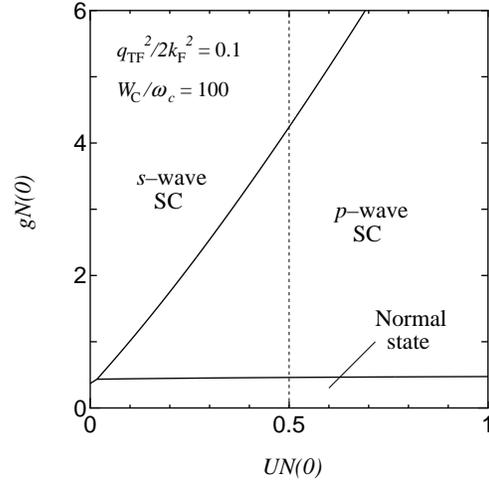
Fig. 13.   The phase diagram for a weak screening case, in which we set $q_{\mathrm{TF}}^2/2k_{\mathrm{F}}^2 = 0.1$ and $W_{\mathrm{C}}/\omega_{\mathrm{c}} = 100$. Along the vertical thin dotted line, the transition temperatures are plotted in Fig. 14.
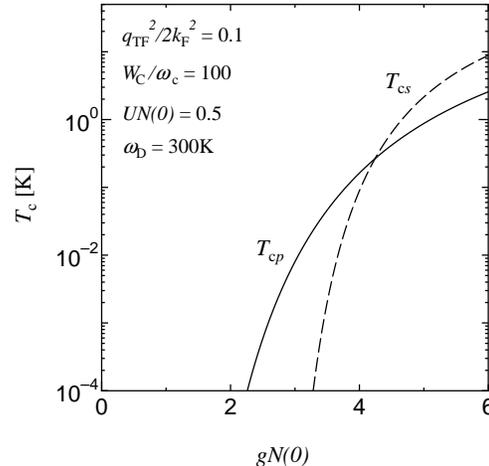
Fig. 14.   The transition temperatures as functions of the effective constant g of the phonon-mediated interaction for a system with the weak screening, in which we set $q_{\mathrm{TF}}^2/2k_{\mathrm{F}}^2 = 0.1$, $W_{\mathrm{C}}/\omega_{\mathrm{c}} = 100$. We have put $\omega_{\mathrm{c}} = 300$ K as an example. The solid and dashed lines show the transition temperatures $T_{\mathrm{c}p}$ and $T_{\mathrm{c}s}$ for the p-wave and s-wave states.

In Fig. 14, the transition termpartures are estimated for the parameter values of Fig. 13. It is found that $T_{\mathrm{c}p}$ for the p-wave state could reach 0.3K, which are practically observable.

6.4   Narrow band systems with weak screening

Lastly, we examine systems with weak Coulomb screening and narrow electron bands. We set parameters as $q_{\mathrm{TF}}^2/2k_{\mathrm{F}}^2 = 0.1$ and $W_{\mathrm{C}}/\omega_{\mathrm{c}} = 20$. The formar corresponds to the Thomas-Fermi screening length
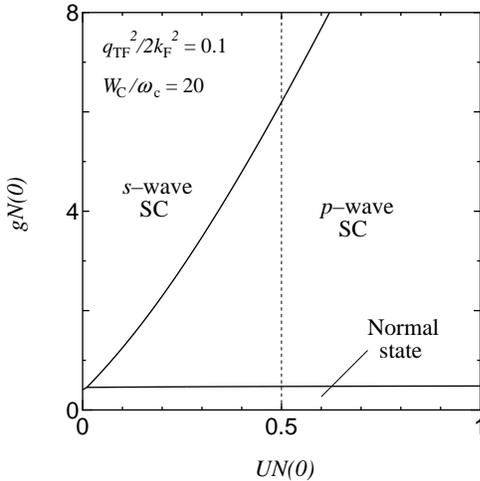
Fig. 15. The phase diagram for a system with weak screening and a narrow electron band, in which we set $q_{\mathrm{TF}}^2/2k_{\mathrm{F}}^2 = 0.1$ and $W_{\mathrm{C}}/\omega_{\mathrm{c}} = 20$. Along the vertical thin dotted line, the transition temperatures are plotted in Fig. 16.

Fig. 16. The transition temperatures as functions of the effective coupling constant g of the phonon-mediated interaction for the system with the weak screening and the narrow electron band, in which we set $q_{\mathrm{TF}}^2/2k_{\mathrm{F}}^2 = 0.1$, $W_{\mathrm{C}}/\omega_{\mathrm{c}} = 20$. We have put $\omega_{\mathrm{c}} = 300$ K as an example. The solid and dashed lines show the transition temperatures $T_{\mathrm{c}p}$ and $T_{\mathrm{c}s}$ for the p-wave and s-wave states.

$\lambda_{\mathrm{TF}} \gtrsim 0.7 \times a$ as mentioned in the previous case. The latter corresponds to $W/\omega_{\mathrm{D}} \sim 2W_{\mathrm{C}}/\omega_{\mathrm{c}} = 40$. If we put $\omega_{\mathrm{D}} = 200 \sim 400$ K as a typical value, we obtain $W = 0.8 \sim 1.6$ eV, which is realistic for the organic superconductors and the ruthenate superconductors. In Figs. 15 and 16, the phase diagram on the U-g plane and the transition temperatures are shown. Comparing Figs. 13 and 15, we confirm again that the area of the triplet state is enlarged when the electron band width becomes narrower. In Fig. 16, we find that the transition temperature $T_{\mathrm{c}p}$ of the triplet state can reach 3 K at $gN(0) \approx 6.2$, although for $gN(0) \gtrsim 6.2$, the p-wave state is hidden behind the s-wave state ($T_{\mathrm{c}s} > T_{\mathrm{c}p}$). We shall discuss the application of this result to the real compounds in the last section.

7. Summary and Discussion

7.1 Summary of the results

Now, we shall summarize the results. In §2, we have derived an effective Hamiltonian which is written in terms of the short-range (on-site) Coulomb interactions U and the long-range Coulomb interactions $v_{\boldsymbol{q}}$, from a basic Hamiltonian. On the basis of this effective Hamiltonian, we have examined the spin and charge fluctuations and screened Coulomb interactions (§3.1), considering the two-particle vertex part within an RPA extended to the model including both U and $v_{\boldsymbol{q}}$. The effective interactions between electrons are written in the simple forms as shown in eqs. (3.11) and (3.12). We have derived an expression of the dielectric function and the screening length (§3.2). It was found that the screening length is lengthened by the on-site correlations due to U.

In §3.3 and §3.4, we have examined the Coulomb screening corrections to the electron-phonon interactions and the phonon Green's function within the RPA consistent with those for the interactions between electrons. It was found that the sound velocity increases by the weakening of the screening due to the on-site correlations mentioned above.

In §4, we have examined superconductivity. We have derived a general form of the effective Hamiltonian which includes the interactions mediated by the phonons and those mediated by the spin and charge fluctuations, where the short and long-range parts of the Coulomb interactions and the screening effects are taken into account. It was found in eq. (4.15) that the effective interaction is written in a summation of two terms, that is, $\Gamma_U^{(0)}$ and the renormalized phonon-mediated pairing interaction. Here, we call $\Gamma_U^{(0)}$ the Hubbard term, because it is nothing but the vertex part in the pure Hubbard model without the long-range Coulomb interaction $v_{\boldsymbol{q}}$. In contrast, the latter term has the same form as the phonon-mediated interaction in the absence of the short-range Coulomb interaction U, but the prefactor and the phonon energy $\tilde{\omega}_{\boldsymbol{q}}$ include the corrections due to U.

In §5, we derived the effective interactions along the same way as the traditional weak coupling theory of superconductivity. In particular, for the system away from any magnetic instability, we derived the effective Hamiltonian, with which we have examined anisotropic superconductivity in §6. The present model includes the models examined so far[5–7,11] in appropriate limits except the corrections due to U.

In §6, we have applied our theory to some ideal sys-

tems. The results are summarized as follows: (1) The triplet superconductivity occurs in the system with strong on-site correlations and weak electron-phonon coupling; (2) Spin-triplet pairing is favored when the band width is narrow and when Coulomb screening is weak;[10] (3) The transition temperature of p-wave pairing is limited, because s-wave pairing is favored if the electron-phonon coupling is strong. In the most favorable system, the transition temperature T_{cp} can be only of the order of 1 K as a crude estimation. These results agree with our knowledge as follows: The triplet superconductivity has not been observed in the ordinary metals, while there are candidates in the heavy fermion superconductors, and the layered superconductors with large layer intervals, such as $(TMTSF)_2X$ and Sr_2RuO_4, but their T_c's are not so high.

7.2   Narrow band width and triplet pairing

As mentioned in the above summary, we have found in Figs. 10 - 12 that p-wave pairing is favored in narrow band systems. This result can be explained as follows. The on-site Coulomb repulsion affects only s-wave pairing, but it has a limit itself. The effective Coulomb parameter μ_0 satisfies an inequality

$$\mu_0^* = \frac{\mu_0}{1 + \mu_0 \ln(W_C/\omega_c)} \lesssim \frac{1}{1 + \ln(W_C/\omega_c)} \equiv \mu_{\max},$$
(7.1)

where we have used $1 > U\chi_0(\boldsymbol{q}, 0) \gtrsim UN(0)$, which is the necessary condition for the absence of the magnetic long-range order within the RPA. The upper bound $\mu_{\max}$ is determined only by the ratio W_C/ω_c, which is usually of the order of W/ω_D. Therefore, we obtain $\mu_{\max} \sim 0.18$, 0.30, and 0.38, for $W_C/\omega_c \sim 100$, 10, and 5, respectively. The phonon-mediated pairing interaction originally has the anisotropic components, such as λ_p, but they are much smaller than the isotropic component λ_s. For triplet pairing to occur only by phonon-mediated pairing interaction, it is needed that s-wave pairing is suppressed for some reason, and the dominancy of the coupling constants, λ_s and λ_p, changes. From the results shown in Fig. 12, the value $\mu_{\max} \sim 0.18$ for $W_C/\omega_c \sim 100$ is too small to change the dominancy, when $\lambda_{TF} \sim 1/k_F$. In contrast, the large value of $\mu_{\max} = 0.30 \sim 0.38$ for $W_C/\omega_c = 10 \sim 5$ can be large enough to suppress the s-wave state.[41]

7.3   Application to the heavy fermion systems

The value of T_c obtained in Fig. 11 is consistent with $T_c \approx 0.5$ K in the heavy fermion UPt_3 system,[29,30] if the set of the parameter values $q_{TF}^2/2k_F^2 = 0.5$ and $W_C/\omega_c = 5$ is regarded to be appropriate for this compound. In addition, as in UGe_2,[8,9] if singlet pairing is suppressed by the internal exchange field due to the co-existing ferromagnetic long-range order, the p-wave transition temperature T_{cp} can be of the order of $1 \sim 2$ K, which is consistent with the experimental value and our

previous result.[7,42]

7.4   Conclusion and future study

In conclusion, we have examined a model of the electron-phonon system with both the long-range and short-range Coulomb interactions, which is derived from a more basic model. In particular, we have examined superconductivity, and shown that the phonon-mediated interaction could induce spin-triplet pairing, when the Coulomb screening is relatively weak and the on-site Coulomb interaction is strong. The transition temperature can be high enough to be observed in practice, and similar to the experimental values in the candidates of the spin-triplet superconductors. In the future, more quantitative study on the isotope effect, in which the correlation effects and the strong coupling effects are taken into account, may give a direct evidence of the applicability of this mechanism.

For more precise estimations of T_{cp} in the application to Sr_2RuO_4 compound, we need to take into account the two-dimensionality. We have examined a two-dimensional effective model in our previous paper,[11] and shown that a realistic value of T_{cp} can be reproduced. It is possible to derive the effective Hamiltonian from the present Hamiltonian with the interaction of eq. (5.4). The derivation will be presented in a separate paper.[43]

The application to the quasi-one-dimensional (Q1D) organic superconductor $(TMTSF)_2X$ is another interesting subject to study as discussed in §1. In particular, Suginishi and the present author found by detailed calculations based on the present theory that specific features of the Q1D system play an important role in the pairing symmetry. It will also be presented in a separate paper.[27]

1) J. R. Schrieffer: *Theory of superconductivity*, pp. 100 (Addison-Weslay, New York, 1983).
2) I. F. Foulkes and B. L. Gyorffy: Phys. Rev. B **15** (1977) 1395.
3) A. A. Abrikosov: Physica C **222** (1994) 191; *ibid* **244** (1995) 243.
4) J. Bouvier and J. Bok: Physica C **249** (1995) 117.
5) J. Friedel and M. Kohmoto: Int. J. Mod. Phys. B **15** (2001) 517.
6) I. Chang, J. Friedel, and M. Kohmoto: Europhys. Lett. **50** (2000) 782.
7) H. Shimahara and M. Kohmoto: Europhys. Lett. **57** (2002) 247.
8) S. S. Saxena, *et al.*: Nature **406** (2000) 587.
9) For UGe₂, a magnetic mechanism has also been proposed in T. R. Kirkpatrick, D. Belitz, T. Vojta, and R. Narayanan: Phys. Rev. Lett. **87** (2001) 127003; T. R. Kirkpatrick and B. Belitz: Phys. Rev. B **67** (2003) 024515.
10) Here, we do not consider the system with extremely weak screening so that such a system becomes an insulating Wigner

lattice.

11) H. Shimahara and M. Kohmoto: Phys. Rev. B **65** (2002) 174502.

12) K. Ishida *et al.*: Nature **396** (1998) 658.

13) G. M. Luke *et al.*: Nature **394** (1998) 558.

14) For a review, see, for example, A. P. Mackenzie and Y. Maeno: Rev. Mod. Phys. **75** (2003) 658.

15) Z. Q. Mao *et al.*: Phys. Rev. B **63** (2001) 144514.

16) H. Shimahara: J. Phys. Soc. Jpn. **72** (2003) 1843.

17) H. Shimahara: J. Phys. Soc. Jpn. **72** (2003) 1851.

18) M. Takigawa, H. Yasuoka, and G. Saito: J. Phys. Soc. Jpn. **56** (1987) 873.

19) Y. Hasegawa and H. Fukuyama: J. Phys. Soc. Jpn. **56** (1987) 877.

20) For a review, see, for example, T. Ishiguro and K. Yamaji: *Organic Superconductors* (Springer, Berlin, Heidelberg, 1990).

21) V. J. Emery: Synth. Met. **13** (1986) 21.

22) H. Shimahara: J. Phys. Soc. Jpn. **58** (1989) 1735.

23) I. J. Lee *et al.*: Phys. Rev. B **68** (2003) 092510; Phys. Rev. Lett. **88** (2002) 017004.

24) J. I. Oh and M. J. Naughton: Phys. Rev. Lett. **92** (2004) 067001.

25) S. Belin and K. Behnia: Phys. Rev. Lett. **79** (1997) 2125.

26) The results of the thermal conductivity in Ref. 25 suggest a full gap state, while the NMR results in Ref. 18 suggest existence of the line nodes. This discrepancy has been discussed in Refs. 44 and 45. It has sometimes been claimed that sufficiently low temperatures to prove the existence of line nodes were not reached in the experiments in Ref. 18. However, at present, there is not any explanation of $T_1^{-1} \sim T^3$ for $T_c \gtrsim T \gtrsim T_c/2$ without line nodes or a nearly line-node-like behavior[44] of the gap function, as far as the author's knowledge.

27) Y. Suginishi and H. Shimahara: unpublished.

28) H. Shimahara: J. Phys. Soc. Jpn. **69** (2000) 1966.

29) For a review, see, for example, M. Sigrist and K. Ueda: Rev. Mod. Phys. **63** (1991) 239.

30) H. Tou, *et al.*: Phys. Rev. Lett. **77** (1996) 1374.

31) The interactions mediated by antiferromagnetic fluctuations include attractive components which contribute to triplet pairing.[22, 28, 35, 36]

32) For a review, see, for example, A. J. Leggett: Rev. Mod. Phys. **47** (1975) 332.

33) The ratios T_{cp}/ϵ_F happen to be of the same order in the Sr_2RuO_4 system and the liquid ^{3}He. One might consider that this suggests an analogy between these systems, but actualy it is only accidental. It is needless to say, the repulsions between electrons and that between ^{3}He atoms are different in their magnitudes and momentum dependences.

34) Note that eq. (2.17) is rotational invariant.

35) D. J. Scalapino, E. Loh, Jr., and J. E. Hirsch: Phys. Rev. B **34** (1986) 8190; K. Miyake, S. Schmitt-Rink, and C. M. Varma: Phys. Rev. B **34** (1986) 6554.

36) H. Shimahara and S. Takada: J. Phys. Soc. Jpn. **57** (1988) 1044.

37) The significance of the self-energy effects on T_c in the spin fluctuation mechanism has been clarified in Ref. 22.

38) N. E. Bickers, D. J. Scalapino, and S. R. White: Phys. Rev. Lett. **62** (1989) 961.

39) K. Yonemitsu: J. Phys. Soc. Jpn. **59** (1990) 2183.

40) For a derivation, see, for example, Refs. 1 and 17.

41) For example, if we put $T_c = 10$ K and $\omega_D = 300$ K, we obtain $\lambda \approx 0.28$ by the weak coupling formula of T_c, which is smaller than $\mu_{max} = 0.30 \sim 0.38$.

42) For the heavy fermion compound UPt$_3$, the value $q_{TF}^2/2k_F^2 = 0.5$ may be considered to be too small, because $q_{TF}^2/2k_F^2 \propto m_b/m$ in eq. (5.31). If we use the effective mass m^* of the heavy fermions as m_b, the factor $m_b/m \sim 180$ for UPt$_3$[46] implies an extremely large value of $q_{TF}^2/2k_F^2$ of the order of 100. However, as discussed in §1, it is obviously an artifact of the Thomas-Fermi approximation and the jellium model. For a practical purpose, it is more appropriate to take a smaller value such as $q_{TF}^2/2k_F^2 = 0.5$, so that an appropriate value of the nearest neighbor Coulomb interaction is reproduced.

43) H. Shimahara: unpublished.

44) H. Shimahara: Phys. Rev. B **61** (2000) R14936.

45) R. W. Cherng and C. A. R. Sá de Melo: Phys. Rev. B **67** (2003) 212505.

46) A. de Visser, A. Menovsky and J. J. M. Franse: Physica B **147** (1987) 81.